Central exclusive diffractive production of $K^+K^-K^+K^-$ via the intermediate $\phi\phi$ state in proton-proton collisions

Piotr Lebiedowicz,[1,*] Otto Nachtmann,[2,†] and Antoni Szczurek[1,‡]

[1]*Institute of Nuclear Physics Polish Academy of Sciences, Radzikowskiego 152, PL-31342 Kraków, Poland*
[2]*Institut für Theoretische Physik, Universität Heidelberg, Philosophenweg 16, D-69120 Heidelberg, Germany*

(Received 8 February 2019; revised manuscript received 25 April 2019; published 24 May 2019)

We present a study of the exclusive $pp \to ppK^+K^-K^+K^-$ reaction at high energies. We consider diffractive mechanisms with the intermediate $\phi\phi$ state with its decay into the $K^+K^-K^+K^-$ system. We include the $\phi(1020)$ $\hat{t}/\hat{u}$-channel exchanges and the $f_2(2340)$ s-channel exchange mechanism. This f_2 state is a candidate for a tensor glueball. We discuss the possibility to use the $pp \to pp\phi\phi$ process in identifying the Odderon exchange. An upper limit for the $\mathbb{P}\mathbb{O}\phi$ coupling is extracted from the WA102 experimental data. The amplitudes for the processes are formulated within the tensor-Pomeron and vector-Odderon approach. We adjust parameters of our model to the WA102 data and present several predictions for the ALICE, ATLAS, CMS, and LHCb experiments. Integrated cross sections of order of a few nb are obtained, including the experimental cuts relevant for the LHC experiments. The distributions in the four-kaon invariant mass, rapidity distance between the two ϕ mesons, special "glueball filter variable," and proton-proton relative azimuthal angle are presented. The distribution in rapidity difference of both ϕ-mesons could shed light on the $f_2(2340) \to \phi\phi$ coupling, not known at present. We discuss the possible role of the $f_0(2100)$, $\eta(2225)$, and $X(2500)$ resonances observed in the $\phi\phi$ channel in radiative decays of J/ψ. Using typical kinematic cuts for LHC experiments, we find from our model that the Odderon-exchange contribution should be distinguishable from other contributions for large rapidity distance between the ϕ mesons and in the region of large four-kaon invariant masses. At least, it should be possible to derive an upper limit on the Odderon contribution in this reaction.

DOI: 10.1103/PhysRevD.99.094034

I. INTRODUCTION

Diffractive studies are one of the important parts of the physics program for the RHIC and LHC experiments. A particularly interesting class is the central-exclusive-production (CEP) processes, where all centrally produced particles are detected; see Sec. 5 of [1]. In recent years, there has been a renewed interest in exclusive production of $\pi^+\pi^-$ pairs at high energies related to successful experiments by the CDF [2] and the CMS [3] collaborations. These measurements are important in the context of resonance production, in particular, in searches for glueballs. The experimental data on central exclusive $\pi^+\pi^-$ production measured at Fermilab and CERN all show visible structures in the $\pi^+\pi^-$ invariant mass. As we discussed in Ref. [4], the pattern of these structures has a mainly resonant origin and is very sensitive to the cuts used in a particular experiment (usually these cuts are different for different experiments). In the CDF and CMS experiments, the large rapidity gaps around the centrally produced dimeson system are checked, but the forward- and backward-going (anti) protons are not detected. Preliminary results of similar CEP studies have been presented by the ALICE [5] and LHCb [6] collaborations at the LHC. Although such results will have a diffractive nature, further efforts are needed to ensure their exclusivity. Ongoing and planned experiments at the RHIC (see, e.g., [7]) and future experiments at the LHC will be able to detect all particles produced in central exclusive processes, including the forward- and backward-going protons. Feasibility studies for the $pp \to pp\pi^+\pi^-$ process with tagging of the scattered protons as carried out for the ATLAS and ALFA detectors are shown in [8]. Similar possibilities exist using the CMS and TOTEM detectors; see, e.g., [9].

It was known for a long time that the frequently used vector-Pomeron model has problems from the point of view of field theory. Taken literally, it gives opposite signs for pp

*Piotr.Lebiedowicz@ifj.edu.pl
†O.Nachtmann@thphys.uni-heidelberg.de
‡Also at Faculty of Mathematics and Natural Sciences, University of Rzeszów, Pigonia 1, PL-35310 Rzeszów, Poland. Antoni.Szczurek@ifj.edu.pl

and $\bar{p}p$ total cross sections. A way to solve these problems was discussed in [10], where the Pomeron was described as a coherent superposition of exchanges with spin $2+4+6+\ldots$. The same idea is realized in the tensor-Pomeron model formulated in [11]. In this model, Pomeron exchange can effectively be treated as the exchange of a rank-2 symmetric tensor. In [12] it was shown that the tensor-Pomeron model is consistent with the experimental data on the helicity structure of proton-proton elastic scattering at $\sqrt{s}=200\,\mathrm{GeV}$ and small $|t|$ from the STAR experiment [13]. In Ref. [14] the tensor-Pomeron model was applied to the diffractive production of several scalar and pseudoscalar mesons in the reaction $pp \to ppM$. In [15] an extensive study of the photoproduction reaction $\gamma p \to \pi^+\pi^- p$ in the framework of the tensor-Pomeron model was presented. The resonant ($\rho^0 \to \pi^+\pi^-$) and nonresonant (Drell-Söding) photon-Pomeron/Reggeon $\pi^+\pi^-$ production in pp collisions was studied in [16]. The central exclusive diffractive production of the $\pi^+\pi^-$ continuum together with the dominant scalar $f_0(500)$, $f_0(980)$, and tensor $f_2(1270)$ resonances was studied by us in [4]. The ρ^0 meson production associated with a very forward/backward πN system in the $pp \to pp\rho^0\pi^0$ and $pp \to pn\rho^0\pi^+$ processes was discussed in [17]. Also the central exclusive $\pi^+\pi^-\pi^+\pi^-$ production via the intermediate $\sigma\sigma$ and $\rho^0\rho^0$ states in pp collisions was considered in [18]. In [19] the $pp \to ppp\bar{p}$ reaction was studied. Recently, in [20], the exclusive diffractive production of the K^+K^- in the continuum and via the dominant scalar $f_0(980)$, $f_0(1500)$, $f_0(1710)$, and tensor $f_2(1270)$, $f_2'(1525)$ resonances, as well as the K^+K^- photoproduction contributions, was discussed in detail. In [21] a possibility to extract the Pomeron-Pomeron-$f_2(1270)$ [$\mathbb{P}\mathbb{P}f_2(1270)$] couplings from the analysis of angular distributions in the $\pi^+\pi^-$ rest system was studied.

The identification of glueballs in the $pp \to pp\pi^+\pi^-$ reaction, being analyzed by the STAR, ALICE, ATLAS, CMS, and LHCb collaborations, can be rather difficult, as the di-pion spectrum is dominated by the $q\bar{q}$ states and mixing of the pure glueball states with nearby $q\bar{q}$ mesons is possible. The partial wave analyses of future experimental data could be used in this context. Studies of different decay channels in central exclusive production would be very valuable. One of the promising reactions is $pp \to pp\phi\phi$ with both $\phi \equiv \phi(1020)$ mesons decaying into the K^+K^- channel. The advantage of this process for experimental studies is the following. The $\phi(1020)$ is a narrow resonance and it can be easily identified in the K^+K^- spectra. On the other hand, non-$\phi\phi$ backgrounds in these spectra should have a broad distribution. However, identification of possible glueball-like states in this channel requires calculation/estimation both of resonant and continuum processes. It is known from the WA102 analysis of various channels that the so-called "glueball-filter variable" ($\mathrm{dP_t}$) [22], defined by the difference of the transverse momentum vectors of the outgoing protons, can be used to select out known $q\bar{q}$ states from non-$q\bar{q}$ candidates. It was observed by the WA102 Collaboration (see, e.g., [23–29]) that all the undisputed $q\bar{q}$ states are suppressed at small $\mathrm{dP_t}$ in contrast to glueball candidates. It is therefore interesting to make a similar study of the $\mathrm{dP_t}$ dependence for the $\phi\phi$ system decaying into $K^+K^-K^+K^-$ in central pp collisions at the LHC.

Structures in the $\phi\phi$ invariant-mass spectrum were observed by several experiments. Broad $J^{PC}=2^{++}$ structures around 2.3 GeV were reported in the inclusive $\pi^- Be \to \phi\phi + X$ reaction [30,31], in the exclusive $\pi^- p \to \phi\phi n$ [32,33] and $K^- p \to \phi\phi\Lambda$ [34,35] reactions, in central production [36–38], and in $p\bar{p}$ annihilations [39]. In the radiative decay $J/\psi \to \gamma\phi\phi$ an enhancement near $\mathrm{M}_{\phi\phi}=2.25$ GeV with preferred $J^{PC}=0^{-+}$ was observed [40–43]. The last partial wave analysis [43] shows that the $\eta(2225)$ state is significant, but a large contribution from the direct decay of $J/\psi \to \gamma\phi\phi$, modeled by a 0^{-+} phase space distribution of the $\phi\phi$ system, was also found there. Also the scalar state $f_0(2100)$ and two additional pseudoscalar states, $\eta(2100)$ and the $X(2500)$, were observed. Three tensor states, $f_2(2010)$, $f_2(2300)$, and $f_2(2340)$, observed previously in [32,33], were also observed in $J/\psi \to \gamma\phi\phi$. It was concluded there that the tensor spectrum is dominated by the $f_2(2340)$. The nature of these resonances is not understood at present and a tensor glueball has still not been clearly identified. According to lattice-QCD simulations, the lightest tensor glueball has a mass between 2.2 and 2.4 GeV; see, e.g., [44–50]. The $f_2(2300)$ and $f_2(2340)$ states are good candidates to be tensor glueballs. For an experimental work indicating a possible tensor glueball, see [51]. Also lattice-QCD predictions for the production rate of the pure gauge tensor glueball in radiative J/ψ decays [52] are consistent with the large production rate of the $f_2(2340)$ in the $\eta\eta$ [53], $\phi\phi$ [43], and $K_S K_S$ [54] channels.

We have presented here some discussion of the role of resonances with masses around 2 GeV in connection with their possible glueball interpretations. With this we want to underline the importance of the study of resonances in this mass range. Our present paper aims to facilitate such studies, for instance, by investigating in detail the interplay of continuum and resonance production of $\phi\phi$ states. But we emphasize that in the following we make no assumptions if the resonances considered are glueballs or not.

In the present paper we wish to concentrate on the CEP of four charged kaons via the intermediate $\phi\phi$ state. Here we shall give explicit expressions for the $pp \to pp\phi\phi$ amplitudes involving the Pomeron-Pomeron fusion to $\phi\phi$ ($\mathbb{P}\mathbb{P} \to \phi\phi$) through the continuum processes, due to the $\hat{t}$- and $\hat{u}$-channel Reggeized ϕ-meson, photon, and Odderon exchanges, as well as through the s-channel resonance reaction [$\mathbb{P}\mathbb{P} \to f_2(2340) \to \phi\phi$]. The pseudoscalar mesons having $I^G=0^+$ and $J^{PC}=0^{-+}$ can also be produced

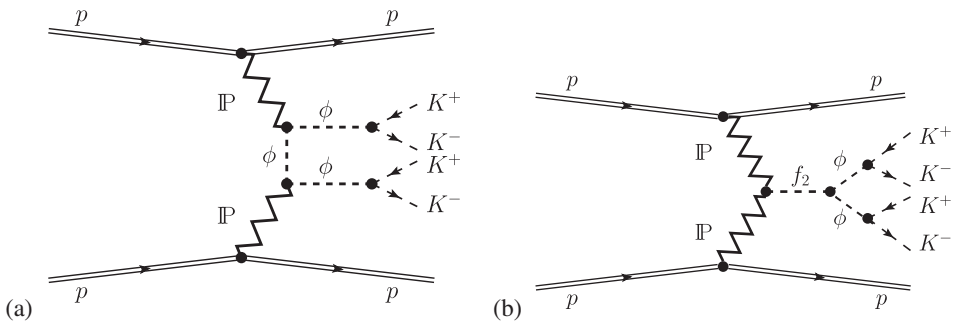

FIG. 1. The "Born-level" diagrams for double Pomeron central exclusive $\phi\phi$ production and their subsequent decays into $K^+K^-K^+K^-$ in proton-proton collisions: (a) continuum $\phi\phi$ production; (b) $\phi\phi$ production via an f_2 resonance. Other resonances, e.g., of f_0- and η-type, can also contribute here.

in Pomeron-Pomeron fusion and may contribute to our reaction if they decay to $\phi\phi$. Possible candidates are, e.g., $\eta(2225)$ and $X(2500)$, which were observed in radiative decays of J/ψ [43]. The same holds for scalar states with $I^G = 0^+$ and $J^{PC} = 0^{++}$, for example, the scalar $f_0(2100)$ meson. We will comment on the possible influence of these contributions for the CEP of $\phi\phi$ pairs. Some model parameters will be determined from the comparison to the WA102 experimental data [27,38]. In order to give realistic predictions we shall include absorption effects calculated at the amplitude level and related to the pp nonperturbative interactions.

II. EXCLUSIVE DIFFRACTIVE PRODUCTION OF FOUR KAONS

In the present paper we consider the $2 \to 6$ process, CEP of four K mesons, with the intermediate $\phi(1020)\phi(1020)$ resonance pair,

$$pp \to pp\phi\phi \to ppK^+K^-K^+K^-. \tag{2.1}$$

In Fig. 1 we show diagrams for this process, which are expected to be the most important ones at high energies since they involve Pomeron exchanges. Figure 1(a) shows the continuum process. In Fig. 1(b) we have the process with intermediate production of an f_2 resonance,

$$pp \to pp(\mathbb{P}\mathbb{P} \to f_2 \to \phi\phi) \to ppK^+K^-K^+K^-. \tag{2.2}$$

In the place of the f_2 we can also have an f_0- and an η-type resonance. That is, we treat effectively the $2 \to 6$ processes (2.1) and (2.2) as arising from the $2 \to 4$ process, the central diffractive production of two vector $\phi(1020)$ mesons in proton-proton collisions.

In Fig. 1(a) we have the exchange of a ϕ or $\phi_{\mathbb{R}}$ Reggeon, depending on the kinematics, as we shall discuss in detail below. In place of the ϕ or $\phi_{\mathbb{R}}$ we can, in principle, also have an ω or $\omega_{\mathbb{R}}$. But these contributions are expected to be very small since the ϕ is nearly a pure $s\bar{s}$ state, the ω nearly a pure $u\bar{u} + d\bar{d}$ state. In the following we shall, therefore, neglect such contributions.

The production of $\phi\phi$ can also occur through diagrams of the type of Fig. 1 but with Reggeons in the place of the Pomerons. For example, in Fig. 1(a) we can replace the Pomerons by $\phi_{\mathbb{R}}$ Reggeons and the intermediate ϕ by a Pomeron. In Fig. 1(b) we can replace one or two Pomerons by one or two $f_{2\mathbb{R}}$ Reggeons. For high energies and central $\phi\phi$ production such Reggeon contributions are expected to be small and we shall not consider them in our present paper. We shall treat in detail the diagrams with Pomeron exchange (Fig. 1) and diagrams involving Odderon and also photon exchange; see Figs. 2 and 4 below.

A resonance produced in Pomeron-Pomeron fusion must have $I^G = 0^+$ and charge conjugation $C = +1$, but it may

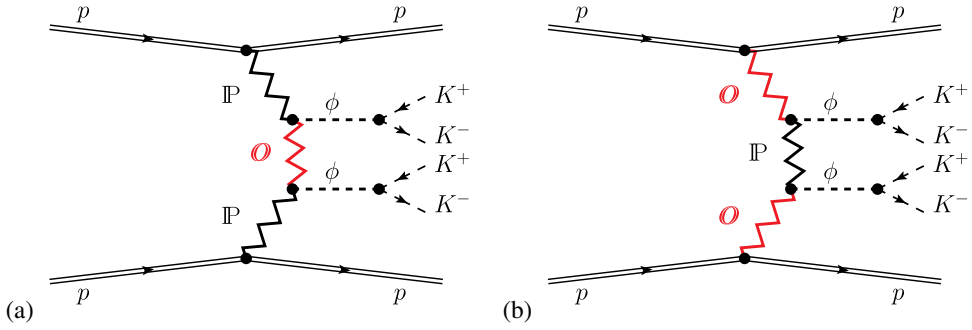

FIG. 2. The Born-level diagrams for diffractive production of a ϕ-meson pair with one and two Odderon exchanges.

TABLE I. A list of resonances, up to a mass of 2500 MeV, that decay into a vector meson pair. The meson masses m and their total widths Γ are taken from PDG [55]. For $\eta(2100)$ and $X(2500)$, the information is taken from [43]. In the first column, the • symbol indicates rather established particles. In the fifth column, the (?) symbol denotes the states that need further experimental confirmation.

Meson	$I^G J^{PC}$	m (MeV)	Γ (MeV)	$\phi\phi$	$K^{*0}\bar{K}^{*0}$	$\rho^0\rho^0$	$\omega\omega$
• $f_1(1285)$	0^+1^{++}	1281.9 ± 0.5	22.7 ± 1.1			Seen	
• $f_0(1370)$	0^+0^{++}	1200–1500	200–500			Dominant	Not seen
• $f_0(1500)$	0^+0^{++}	1504 ± 6	109 ± 7			Seen	
$f_2(1565)$	0^+2^{++}	1562 ± 13	134 ± 8			Seen	Seen
$f_2(1640)$	0^+2^{++}	1639 ± 6	99^{+60}_{-40}				Seen
• $f_0(1710)$	0^+0^{++}	1723^{+6}_{-5}	139 ± 8				Seen
$\eta(1760)$	0^+0^{-+}	1751 ± 15	240 ± 30			Seen	Seen
$f_2(1910)$	0^+2^{++}	1903 ± 9	196 ± 31			Seen	Seen
• $f_2(1950)$	0^+2^{++}	1944 ± 12	472 ± 18		Seen		
• $f_2(2010)$	0^+2^{++}	2011^{+60}_{-80}	202 ± 60	Seen			
$f_0(2020)$	0^+0^{++}	1992 ± 16	442 ± 60			Seen	Seen
$f_0(2100)$	0^+0^{++}	2101 ± 7	224^{+23}_{-21}	Seen (?)			
$\eta(2100)$	0^+0^{-+}	2050^{+30+75}_{-24-26} [43]	$250^{+36+181}_{-30-164}$ [43]	Seen (?)			
• $f_4(2050)$	0^+4^{++}	2018 ± 11	237 ± 18				Seen
$f_J(2220)$	$0^+(2^{++}$ or $4^{++})$	2231.1 ± 3.5	23^{+8}_{-7}	Not seen			
$\eta(2225)$	0^+0^{-+}	2221^{+13}_{-10}	185^{+40}_{-20}	Seen (?)			
• $f_2(2300)$	0^+2^{++}	2297 ± 28	149 ± 40	Seen			
$f_4(2300)$	0^+4^{++}	2320 ± 60	250 ± 80			Seen	Seen
• $f_2(2340)$	0^+2^{++}	2345^{+50}_{-40}	322^{+70}_{-60}	Seen			
$X(2500)$	0^+0^{-+}	$2470^{+15+101}_{-19-23}$ [43]	230^{+64+56}_{-35-33} [43]	Seen (?)			

have various spin and parity quantum numbers. See, e.g., the discussion in Appendix A of [14].

In Table I we have listed intermediate resonances that can contribute to the $pp \to pp\phi\phi$ reaction (2.2) and to other processes with two vector mesons in the final state. It must be noted that the scalar state $f_0(2100)$ and three pseudoscalar states, $\eta(2100)$, $\eta(2225)$, and $X(2500)$, which were observed in the process $J/\psi \to \gamma\phi\phi$ [43], are only listed in PDG [55] and are not included in the summary tables. Clearly these states need confirmation.

To calculate the total cross section for the $2 \to 4$ reactions one has to calculate the 8-dimensional phase-space integral[1] numerically [56]. Some modifications of the $2 \to 4$ reaction are needed to simulate the $2 \to 6$ reaction with $K^+K^-K^+K^-$ in the final state. For example, since the $\phi(1020)$ is an unstable particle one has to include a smearing of the ϕ masses due to their resonance distribution. Then, the general cross-section formula can be written approximately as

$$\sigma_{2\to 6} = [\mathcal{B}(\phi(1020) \to K^+K^-)]^2 \times \int_{2m_K}^{\max\{m_{X_3}\}} \int_{2m_K}^{\max\{m_{X_4}\}} \sigma_{2\to 4}(\ldots, m_{X_3}, m_{X_4}) \times f_\phi(m_{X_3}) f_\phi(m_{X_4}) dm_{X_3} dm_{X_4}, \tag{2.3}$$

with the branching fraction $\mathcal{B}(\phi(1020) \to K^+K^-) = 0.492$ [55]. We use for the calculation of the decay process $\phi(1020) \to K^+K^-$ the spectral function

$$f_\phi(m_{X_i}) = C_\phi \left(1 - \frac{4m_K^2}{m_{X_i}^2}\right)^{3/2} \frac{\frac{2}{\pi} m_\phi^2 \Gamma_\phi}{(m_{X_i}^2 - m_\phi^2)^2 + m_\phi^2 \Gamma_\phi^2}, \tag{2.4}$$

where $i = 3, 4$, Γ_ϕ is the total width of the $\phi(1020)$ resonance, m_ϕ its mass, and $C_\phi = 64.1$ is found from the condition

$$\int_{2m_K}^{\infty} f_\phi(m_{X_i}) dm_{X_i} = 1. \tag{2.5}$$

The quantity $(1 - 4m_K^2/m_{X_i}^2)^{3/2}$ smoothly decreases the spectral function when approaching the K^+K^- threshold, $m_{X_i} \to 2m_K$, and takes into account the angular momentum $l = 1$ of the K^+K^- state.

To include experimental cuts on charged kaons we perform the decays of ϕ mesons isotropically[2] in the ϕ rest frames and then use relativistic transformations to the overall center-of-mass frame.

[1] In the integration over four-body phase space, the transverse momenta of the produced particles (p_{1t}, p_{2t}, p_{3t}, p_{4t}); the azimuthal angles of the outgoing protons (ϕ_1, ϕ_2); and the rapidities of the produced mesons (y_3, y_4) were chosen as integration variables over the phase space.

[2] This is true for unpolarized ϕ's. In principle our model also makes predictions for the polarization of the ϕ's and the anisotropies of the resulting K^+K^- decay distributions. Once a good event generator for our reaction is available, all of these effects should be included.

In principle, there are other processes contributing to the $K^+K^-K^+K^-$ final state, for example, direct $K^+K^-K^+K^-$ continuum production and processes with $f_{0,2}$ resonances:

$$pp \to ppK^+K^-K^+K^-, \tag{2.6}$$

$$pp \to ppf_{0,2}K^+K^- \to ppK^+K^-K^+K^-, \tag{2.7}$$

$$pp \to ppf_{0,2}f_{0,2} \to ppK^+K^-K^+K^-, \tag{2.8}$$

$$pp \to pp(f_2 \to f_0 f_0) \to ppK^+K^-K^+K^-. \tag{2.9}$$

Here $f_{0,2}$ stands for one of the scalar or tensor mesons decaying to K^+K^-. It should be noted that a complete theoretical model of the $pp \to ppK^+K^-K^+K^-$ process should include interference effects of the processes (2.1), (2.2), and (2.6)–(2.9). However, such a detailed study of the $pp \to ppK^+K^-K^+K^-$ reaction will only be necessary once high-energy experimental data for the purely exclusive measurements will be available. We leave this interesting problem for future studies. The GenEx Monte Carlo generator [57,58] could be used in this context. We refer the reader to Ref. [59] where a first calculation of four-pion continuum production in the $pp \to pp\pi^+\pi^-\pi^+\pi^-$ reaction with the help of the GenEx code was performed.

III. THE REACTION $pp \to pp\phi\phi$

Here we discuss the exclusive production of $\phi\phi \equiv \phi(1020)\phi(1020)$ in proton-proton collisions,

$$p(p_a,\lambda_a) + p(p_b,\lambda_b) \to p(p_1,\lambda_1) + \phi(p_3,\lambda_3) + \phi(p_4,\lambda_4) + p(p_2,\lambda_2), \tag{3.1}$$

where $p_{a,b}$, $p_{1,2}$ and $\lambda_{a,b}$, $\lambda_{1,2} = \pm\frac{1}{2}$ denote the four-momenta and helicities of the protons and $p_{3,4}$ and $\lambda_{3,4} = 0, \pm 1$ denote the four-momenta and helicities of the ϕ mesons, respectively.

The amplitude for the reaction (3.1) can be written as

$$\mathcal{M}_{\lambda_a\lambda_b\to\lambda_1\lambda_2\phi\phi} = (\epsilon^{(\phi)}_{\rho_3}(\lambda_3))^*(\epsilon^{(\phi)}_{\rho_4}(\lambda_4))^*\mathcal{M}^{\rho_3\rho_4}_{\lambda_a\lambda_b\to\lambda_1\lambda_2\phi\phi}, \tag{3.2}$$

where $\epsilon^{(\phi)}_\mu(\lambda)$ are the polarization vectors of the ϕ meson.

We consider here unpolarized protons in the initial state and no observation of polarizations in the final state. Therefore, we have to insert in (2.3) the cross section $\sigma_{2\to4}$ summed over the ϕ meson polarizations. The spin sum for a ϕ meson of momentum k and squared mass $k^2 = m_X^2$ is

$$\sum_{\lambda=0,\pm1} \epsilon^{(\phi)\mu}(\lambda)(\epsilon^{(\phi)\nu}(\lambda))^* = -g^{\mu\nu} + \frac{k^\mu k^\nu}{m_X^2}. \tag{3.3}$$

But in our model the $k^\mu k^\nu$ terms do not contribute to the cross section since we have the relations

$$p_{3\rho_3}\mathcal{M}^{\rho_3\rho_4}_{\lambda_a\lambda_b\to\lambda_1\lambda_2\phi\phi} = 0, \qquad p_{4\rho_4}\mathcal{M}^{\rho_3\rho_4}_{\lambda_a\lambda_b\to\lambda_1\lambda_2\phi\phi} = 0, \tag{3.4}$$

which will be shown below in Secs. III A and III B.

Taking also into account the statistical factor $\frac{1}{2}$ due to the identity of the two ϕ mesons we get for the amplitudes squared [to be inserted in $\sigma_{2\to4}$ in (2.3)]

$$\frac{1}{2}\frac{1}{4}\sum_{\text{spins}}|\mathcal{M}_{\lambda_a\lambda_b\to\lambda_1\lambda_2\phi\phi}|^2 = \frac{1}{8}\sum_{\lambda_a,\lambda_b,\lambda_1,\lambda_2}(\mathcal{M}^{\sigma_3\sigma_4}_{\lambda_a\lambda_b\to\lambda_1\lambda_2\phi\phi})^*\mathcal{M}^{\rho_3\rho_4}_{\lambda_a\lambda_b\to\lambda_1\lambda_2\phi\phi}g_{\sigma_3\rho_3}g_{\sigma_4\rho_4}. \tag{3.5}$$

To give the full physical amplitude for the $pp \to pp\phi\phi$ reaction we include absorptive corrections to the Born amplitudes discussed below. For the details of how to include the pp-rescattering corrections in the eikonal approximation for the four-body reaction, see Sec. 3.3 of [16].

A. ϕ-meson exchange mechanism

The diagram for the $\phi\phi$ production with an intermediate ϕ-meson exchange is shown in Fig. 1(a). The Born-level amplitude can be written as the sum

$$\mathcal{M}^{(\phi\text{-exchange})\rho_3\rho_4}_{\lambda_a\lambda_b\to\lambda_1\lambda_2\phi\phi} = \mathcal{M}^{(\hat{t})\rho_3\rho_4}_{\lambda_a\lambda_b\to\lambda_1\lambda_2\phi\phi} + \mathcal{M}^{(\hat{u})\rho_3\rho_4}_{\lambda_a\lambda_b\to\lambda_1\lambda_2\phi\phi}, \tag{3.6}$$

with the $\hat{t}$- and $\hat{u}$-channel amplitudes:

$$\mathcal{M}^{(\hat{t})}_{\rho_3\rho_4} = (-i)\bar{u}(p_1,\lambda_1)i\Gamma^{(\mathbb{P}pp)}_{\mu_1\nu_1}(p_1,p_a)u(p_a,\lambda_a)i\Delta^{(\mathbb{P})\mu_1\nu_1,\alpha_1\beta_1}(s_{13},t_1)i\Gamma^{(\mathbb{P}\phi\phi)}_{\rho_1\rho_3\alpha_1\beta_1}(\hat{p}_t,-p_3)i\Delta^{(\phi)\rho_1\rho_2}(\hat{p}_t)i\Gamma^{(\mathbb{P}\phi\phi)}_{\rho_4\rho_2\alpha_2\beta_2}(p_4,\hat{p}_t) \times i\Delta^{(\mathbb{P})\alpha_2\beta_2,\mu_2\nu_2}(s_{24},t_2)\bar{u}(p_2,\lambda_2)i\Gamma^{(\mathbb{P}pp)}_{\mu_2\nu_2}(p_2,p_b)u(p_b,\lambda_b), \tag{3.7}$$

$$\mathcal{M}^{(\hat{u})}_{\rho_3\rho_4} = (-i)\bar{u}(p_1,\lambda_1)i\Gamma^{(\mathbb{P}pp)}_{\mu_1\nu_1}(p_1,p_a)u(p_a,\lambda_a)i\Delta^{(\mathbb{P})\mu_1\nu_1,\alpha_1\beta_1}(s_{14},t_1)i\Gamma^{(\mathbb{P}\phi\phi)}_{\rho_4\rho_1\alpha_1\beta_1}(p_4,\hat{p}_u)i\Delta^{(\phi)\rho_1\rho_2}(\hat{p}_u)i\Gamma^{(\mathbb{P}\phi\phi)}_{\rho_2\rho_3\alpha_2\beta_2}(\hat{p}_u,-p_3) \times i\Delta^{(\mathbb{P})\alpha_2\beta_2,\mu_2\nu_2}(s_{23},t_2)\bar{u}(p_2,\lambda_2)i\Gamma^{(\mathbb{P}pp)}_{\mu_2\nu_2}(p_2,p_b)u(p_b,\lambda_b), \tag{3.8}$$

where $\hat{p}_t = p_a - p_1 - p_3$, $\hat{p}_u = p_4 - p_a + p_1$, $s_{ij} = (p_i + p_j)^2$, $t_1 = (p_1 - p_a)^2$, and $t_2 = (p_2 - p_b)^2$. Here $\Delta^{(\mathbb{P})}$ and $\Gamma^{(\mathbb{P}pp)}$ denote the effective propagator and proton vertex function, respectively, for the tensorial Pomeron. The corresponding expressions, as given in Sec. 3 of [11], are as follows:

$$i\Delta^{(\mathbb{P})}_{\mu\nu,\kappa\lambda}(s,t) = \frac{1}{4s}\left(g_{\mu\kappa}g_{\nu\lambda} + g_{\mu\lambda}g_{\nu\kappa} - \frac{1}{2}g_{\mu\nu}g_{\kappa\lambda}\right)(-is\alpha'_{\mathbb{P}})^{\alpha_{\mathbb{P}}(t)-1}, \tag{3.9}$$

$$i\Gamma^{(\mathbb{P}pp)}_{\mu\nu}(p',p) = -i3\beta_{\mathbb{P}NN}F_1(t)\left\{\frac{1}{2}[\gamma_\mu(p'+p)_\nu + \gamma_\nu(p'+p)_\mu] - \frac{1}{4}g_{\mu\nu}(\not{p}' + \not{p})\right\}, \tag{3.10}$$

where $\beta_{\mathbb{P}NN} = 1.87\ \mathrm{GeV}^{-1}$. For extensive discussions of the properties of these terms we refer to [11]. Here the Pomeron trajectory $\alpha_{\mathbb{P}}(t)$ is assumed to be of standard linear form (see, e.g., [60,61]):

$$\begin{aligned}\alpha_{\mathbb{P}}(t) &= \alpha_{\mathbb{P}}(0) + \alpha'_{\mathbb{P}}t,\\ \alpha_{\mathbb{P}}(0) &= 1.0808, \qquad \alpha'_{\mathbb{P}} = 0.25\ \mathrm{GeV}^{-2}.\end{aligned} \tag{3.11}$$

Our ansatz for the $\mathbb{P}\phi\phi$ vertex follows the one for the $\mathbb{P}\rho\rho$ in (3.47) of [11] with the replacements $a_{\mathbb{P}\rho\rho} \to a_{\mathbb{P}\phi\phi}$ and $b_{\mathbb{P}\rho\rho} \to b_{\mathbb{P}\phi\phi}$. This was already used in Sec. IV B of [20]. The $\mathbb{P}\phi\phi$ vertex function is taken with the same Lorentz structure as for $f_2\gamma\gamma$ defined in (3.39) of [11]. With k', μ and k, ν the momentum and vector index of the outgoing and incoming ϕ, respectively, and $\kappa\lambda$ the Pomeron indices, the $\mathbb{P}\phi\phi$ vertex reads

$$i\Gamma^{(\mathbb{P}\phi\phi)}_{\mu\nu\kappa\lambda}(k',k) = iF_M((k'-k)^2)[2a_{\mathbb{P}\phi\phi}\Gamma^{(0)}_{\mu\nu\kappa\lambda}(k',-k) - b_{\mathbb{P}\phi\phi}\Gamma^{(2)}_{\mu\nu\kappa\lambda}(k',-k)], \tag{3.12}$$

with two rank-four tensor functions,

$$\Gamma^{(0)}_{\mu\nu\kappa\lambda}(k_1,k_2) = [(k_1\cdot k_2)g_{\mu\nu} - k_{2\mu}k_{1\nu}]\left[k_{1\kappa}k_{2\lambda} + k_{2\kappa}k_{1\lambda} - \frac{1}{2}(k_1\cdot k_2)g_{\kappa\lambda}\right], \tag{3.13}$$

$$\begin{aligned}\Gamma^{(2)}_{\mu\nu\kappa\lambda}(k_1,k_2) &= (k_1\cdot k_2)(g_{\mu\kappa}g_{\nu\lambda} + g_{\mu\lambda}g_{\nu\kappa}) + g_{\mu\nu}(k_{1\kappa}k_{2\lambda} + k_{2\kappa}k_{1\lambda}) - k_{1\nu}k_{2\lambda}g_{\mu\kappa}\\ &\quad - k_{1\nu}k_{2\kappa}g_{\mu\lambda} - k_{2\mu}k_{1\lambda}g_{\nu\kappa} - k_{2\mu}k_{1\kappa}g_{\nu\lambda} - [(k_1\cdot k_2)g_{\mu\nu} - k_{2\mu}k_{1\nu}]g_{\kappa\lambda};\end{aligned} \tag{3.14}$$

see Eqs. (3.18) and (3.19) of [11]. In (3.12) the coupling parameters $a_{\mathbb{P}\phi\phi}$ and $b_{\mathbb{P}\phi\phi}$ have dimensions GeV^{-3} and GeV^{-1}, respectively. In [20] we have fixed the coupling parameters of the tensor Pomeron to the ϕ meson based on the HERA experimental data for the $\gamma p \to \phi p$ reaction [62,63]. We take the coupling constants $a_{\mathbb{P}\phi\phi} = 0.49\ \mathrm{GeV}^{-3}$ and $b_{\mathbb{P}\phi\phi} = 4.27\ \mathrm{GeV}^{-1}$ from Table II of [20] (see also Sec. IV B there).

In the hadronic vertices we should take into account form factors since the hadrons are extended objects. The form factors $F_1(t)$ in (3.10) and $F_M(t)$ in (3.12) are chosen here as the electromagnetic form factors only for simplicity,

$$F_1(t) = \frac{4m_p^2 - 2.79t}{(4m_p^2 - t)(1 - t/m_D^2)^2}, \tag{3.15}$$

$$F_M(t) = \frac{1}{1 - t/\Lambda_0^2}; \tag{3.16}$$

see Eqs. (3.29) and (3.34) of [11], respectively. In (3.15) m_p is the proton mass and $m_D^2 = 0.71\ \mathrm{GeV}^2$ is the dipole mass squared. As we discussed in Fig. 6 of [20] we should take in (3.16) $\Lambda_0^2 = 1.0\ \mathrm{GeV}^2$ instead of $\Lambda_0^2 = 0.5\ \mathrm{GeV}^2$ used for the $\mathbb{P}\rho\rho$ vertex in [11].

Then, with the expressions for the propagators, vertices, and form factors, from [11] $\mathcal{M}^{\rho_3\rho_4}$ can be written in the high-energy approximation as

$$\begin{aligned}\mathcal{M}^{(\phi\text{-exchange})\rho_3\rho_4}_{\lambda_a\lambda_b\to\lambda_1\lambda_2\phi\phi} &= 2(p_1+p_a)_{\mu_1}(p_1+p_a)_{\nu_1}\delta_{\lambda_1\lambda_a}F_1(t_1)F_M(t_1)\\ &\quad\times\{V^{\rho_3\rho_1\mu_1\nu_1}(s_{13},t_1,\hat{p}_t,p_3)\Delta^{(\phi)}_{\rho_1\rho_2}(\hat{p}_t)V^{\rho_4\rho_2\mu_2\nu_2}(s_{24},t_2,-\hat{p}_t,p_4)[\hat{F}_\phi(\hat{p}_t^2)]^2\\ &\quad + V^{\rho_4\rho_1\mu_1\nu_1}(s_{14},t_1,-\hat{p}_u,p_4)\Delta^{(\phi)}_{\rho_1\rho_2}(\hat{p}_u)V^{\rho_3\rho_2\mu_2\nu_2}(s_{23},t_2,\hat{p}_u,p_3)[\hat{F}_\phi(\hat{p}_u^2)]^2\}\\ &\quad\times 2(p_2+p_b)_{\mu_2}(p_2+p_b)_{\nu_2}\delta_{\lambda_2\lambda_b}F_1(t_2)F_M(t_2),\end{aligned} \tag{3.17}$$

where $V_{\mu\nu\kappa\lambda}$ reads as

$$V_{\mu\nu\kappa\lambda}(s,t,k_2,k_1) = \frac{1}{4s}3\beta_{\mathbb{P}NN}(-is\alpha'_{\mathbb{P}})^{\alpha_{\mathbb{P}}(t)-1} \times [2a_{\mathbb{P}\phi\phi}\Gamma^{(0)}_{\mu\nu\kappa\lambda}(k_1,k_2) - b_{\mathbb{P}\phi\phi}\Gamma^{(2)}_{\mu\nu\kappa\lambda}(k_1,k_2)]. \quad (3.18)$$

The amplitude (3.17) contains a form factor $\hat{F}_\phi(\hat{p}^2)$ taking into account the off-shell dependencies of the intermediate ϕ-mesons. The form factor is normalized to unity at the on-shell point $\hat{F}_\phi(m_\phi^2) = 1$ and parametrized here in the exponential form,

$$\hat{F}_\phi(\hat{p}^2) = \exp\left(\frac{\hat{p}^2 - m_\phi^2}{\Lambda^2_{\text{off},E}}\right), \quad (3.19)$$

where the cutoff parameter $\Lambda_{\text{off},E}$ could be adjusted to experimental data.

The relations (3.4) are now easily checked from (3.17) and (3.18) using the properties of the tensorial functions (3.13) and (3.14); see (3.21) of [11]. We can then make in (3.17) the following replacement for the ϕ-meson propagator:

$$\Delta^{(\phi)}_{\rho_1\rho_2}(\hat{p}) \to -g_{\rho_1\rho_2}\Delta^{(\phi)}_T(\hat{p}^2), \quad (3.20)$$

where we take for $\hat{p}^2 < 0$, where $\Delta^{(\phi)}_T(\hat{p}^2)$ must be real, the simple lowest order expression $(\Delta^{(\phi)}_T(\hat{p}^2))^{-1} = \hat{p}^2 - m_\phi^2$.

We should take into account the fact that the exchanged intermediate object is not a simple spin-1 particle (ϕ meson) but may correspond to a Regge exchange; that is, the Reggeization of the intermediate ϕ meson is necessary (see, e.g., [18]). A simple way to include approximately the "Reggeization" of the amplitude given in Eq. (3.17) is by replacing the ϕ-meson propagator in both the $\hat{t}$- and $\hat{u}$-channel amplitudes by

$$\Delta^{(\phi)}_{\rho_1\rho_2}(\hat{p}) \to \Delta^{(\phi)}_{\rho_1\rho_2}(\hat{p})\left(\exp(i\phi(s_{34}))\frac{s_{34}}{s_{\text{thr}}}\right)^{\alpha_\phi(\hat{p}^2)-1}, \quad (3.21)$$

where

$$s_{34} = (p_3+p_4)^2 = \mathrm{M}^2_{\phi\phi}, \qquad s_{\text{thr}} = 4m_\phi^2. \quad (3.22)$$

Here we assume for the ϕ Regge trajectory

$$\alpha_\phi(\hat{p}^2) = \alpha_\phi(0) + \alpha'_\phi\hat{p}^2, \qquad \alpha_\phi(0) = 0.1, \quad \alpha'_\phi = 0.9\ \text{GeV}^{-2}; \quad (3.23)$$

see Eq. (5.3.1) of [64]. In order to have the correct phase behavior we introduced in (3.21) the function $\exp(i\phi(s_{34}))$ with

$$\phi(s_{34}) = \frac{\pi}{2}\exp\left(\frac{s_{\text{thr}} - s_{34}}{s_{\text{thr}}}\right) - \frac{\pi}{2}. \quad (3.24)$$

This procedure of Reggeization assures agreement with mesonic physics in the $\phi\phi$ system close to threshold, $s_{34} = 4m_\phi^2$ (no suppression), and it gives the Regge behavior at large s_{34}. However, some care is needed here, as the Reggeization is only expected in general to hold in the $|\hat{p}^2|/s_{34} \ll 1$ regime. In the reaction considered, both $\langle -\hat{p}_t^2\rangle$ and $\langle -\hat{p}_u^2\rangle$ are of order 1 GeV^2 (before Reggeization) with a cutoff for higher $|\hat{p}^2|$ provided in (3.17) by the form factors $\hat{F}_\phi(\hat{p}^2)$ (3.19). Therefore, the propagator form in (3.21) and (3.24) gives correct Regge behavior for $s_{34} - 4m_\phi^2 \gg 1$ GeV^2 and $|\hat{p}^2|$ limited by the form factors, whereas for smaller s_{34} we have mesonic behavior.

In Ref. [65] it was argued that the Reggeization should not be applied when the rapidity distance between two centrally produced mesons, $\mathrm{Y}_{\text{diff}} = \mathrm{Y}_3 - \mathrm{Y}_4$, tends to zero (i.e., for $|\hat{p}^2| \sim s_{34}$). Indeed, for small Y_{diff} the two ϕ mesons may have large transverse momenta leading to a large $\mathrm{M}_{\phi\phi}$. Clearly this kinematic region has nothing to do with the Regge limit. For large Y_{diff}, on the other hand, the form factors $\hat{F}_\phi(\hat{p}^2)$ in (3.17) limit the transverse momenta of the ϕ's but $\mathrm{M}_{\phi\phi}$ will be large. That is, there we are in the Regge limit. To take care of these two different regimes we propose to use, as an alternative to (3.21), a formula for the ϕ propagator which interpolates continuously between the regions of low Y_{diff}, where we use the standard ϕ propagator, and of high Y_{diff}, where we use the Reggeized form (3.21):

$$\Delta^{(\phi)}_{\rho_1\rho_2}(\hat{p}) \to \Delta^{(\phi)}_{\rho_1\rho_2}(\hat{p})F(\mathrm{Y}_{\text{diff}}) + \Delta^{(\phi)}_{\rho_1\rho_2}(\hat{p})[1 - F(\mathrm{Y}_{\text{diff}})] \times \left(\exp(i\phi(s_{34}))\frac{s_{34}}{s_{\text{thr}}}\right)^{\alpha_\phi(\hat{p}^2)-1}, \quad (3.25)$$

with a simple function

$$F(\mathrm{Y}_{\text{diff}}) = \exp\left(-\mathrm{c_y}|\mathrm{Y}_{\text{diff}}|\right). \quad (3.26)$$

Here $\mathrm{c_y}$ is an unknown parameter which measures how fast one approaches to the Regge regime.

In Sec. IV below we shall compare the two prescriptions of Reggeization, (3.21) and (3.25); see Figs. 6 and 10. Furthermore, we shall show in Fig. 12 that a large size of the rapidity gap between the two ϕ mesons indeed means automatically also large $\mathrm{M}_{\phi\phi}$ in our model.

B. f_2 resonance production

Now we consider the amplitude for the reaction (3.1) through the s-channel f_2-meson exchange as shown in Fig. 1(b). The $f_2(2010)$, $f_2(2300)$, and $f_2(2340)$ mesons could be considered as potential candidates; see Table I.

The Born amplitude for the $\mathbb{PP}$ fusion is given by

$$\begin{aligned}\mathcal{M}^{(\mathbb{PP}\to f_2\to\phi\phi)\rho_3\rho_4}_{\lambda_a\lambda_b\to\lambda_1\lambda_2\phi\phi} &= (-i)\bar{u}(p_1,\lambda_1)i\Gamma^{(\mathbb{P}pp)\mu_1\nu_1}(p_1,p_a)u(p_a,\lambda_a)i\Delta^{(\mathbb{P})}_{\mu_1\nu_1,\alpha_1\beta_1}(s_1,t_1)\\ &\times i\Gamma^{(\mathbb{PP}f_2)\alpha_1\beta_1,\alpha_2\beta_2,\rho\sigma}(q_1,q_2)i\Delta^{(f_2)}_{\rho\sigma,\alpha\beta}(p_{34})i\Gamma^{(f_2\phi\phi)\alpha\beta\rho_3\rho_4}(p_3,p_4)\\ &\times i\Delta^{(\mathbb{P})}_{\alpha_2\beta_2,\mu_2\nu_2}(s_2,t_2)\bar{u}(p_2,\lambda_2)i\Gamma^{(\mathbb{P}pp)\mu_2\nu_2}(p_2,p_b)u(p_b,\lambda_b),\end{aligned}\tag{3.27}$$

where $s_1=(p_1+p_3+p_4)^2$, $s_2=(p_2+p_3+p_4)^2$, $q_1=p_a-p_1$, $q_2=p_b-p_2$, $t_1=q_1^2$, $t_2=q_2^2$, and $p_{34}=q_1+q_2=p_3+p_4$.

The $\mathbb{PP}f_2$ vertex, including a form factor, can be written as

$$i\Gamma^{(\mathbb{PP}f_2)}_{\mu\nu,\kappa\lambda,\rho\sigma}(q_1,q_2)=\left(i\Gamma^{(\mathbb{PP}f_2)(1)}_{\mu\nu,\kappa\lambda,\rho\sigma}|_{\text{bare}}+\sum_{j=2}^{7}i\Gamma^{(\mathbb{PP}f_2)(j)}_{\mu\nu,\kappa\lambda,\rho\sigma}(q_1,q_2)|_{\text{bare}}\right)\tilde{F}^{(\mathbb{PP}f_2)}(q_1^2,q_2^2,p_{34}^2).\tag{3.28}$$

Here and throughout our paper the label "bare" is used for a vertex, as derived from a corresponding coupling Lagrangian [4], without a form-factor function. A possible choice for the $i\Gamma^{(\mathbb{PP}f_2)(j)}_{\mu\nu,\kappa\lambda,\rho\sigma}|_{\text{bare}}$ coupling terms $j=1,\ldots,7$ is given in Appendix A of [4]. The corresponding coupling constants $g^{(j)}_{\mathbb{PP}f_2}$ are not known and should be fitted to existing and future experimental data. In the following we shall, for the purpose of orientation, assume that only $g^{(1)}_{\mathbb{PP}f_2}$ is unequal to zero. But we have checked that for the distributions studied here the choice of $\mathbb{PP}f_2$ coupling is not important; see Sec. IV A below.

In practical calculations, to describe the off-shell dependence in (3.28), we take the factorized form for the $\mathbb{PP}f_2$ form factor,

$$\tilde{F}^{(\mathbb{PP}f_2)}(q_1^2,q_2^2,p_{34}^2)=\tilde{F}_M(q_1^2)\tilde{F}_M(q_2^2)F^{(\mathbb{PP}f_2)}(p_{34}^2),\tag{3.29}$$

normalized to $\tilde{F}^{(\mathbb{PP}f_2)}(0,0,m_{f_2}^2)=1$. We will further set

$$\tilde{F}_M(t)=\frac{1}{1-t/\tilde{\Lambda}_0^2},\qquad \tilde{\Lambda}_0^2=1\ \text{GeV}^2;\tag{3.30}$$

$$F^{(\mathbb{PP}f_2)}(p_{34}^2)=\exp\left(\frac{-(p_{34}^2-m_{f_2}^2)^2}{\Lambda_{f_2}^4}\right),\qquad \Lambda_{f_2}=1\ \text{GeV}.\tag{3.31}$$

For the $f_2\phi\phi$ vertex we take the following ansatz [in analogy to the $f_2\gamma\gamma$ vertex; see (3.39) of [11]]:

$$\begin{aligned}i\Gamma^{(f_2\phi\phi)}_{\mu\nu\kappa\lambda}(p_3,p_4) &= i\frac{2}{M_0^3}g'_{f_2\phi\phi}\Gamma^{(0)}_{\mu\nu\kappa\lambda}(p_3,p_4)F'^{(f_2\phi\phi)}(p_{34}^2)\\ &\quad -i\frac{1}{M_0}g''_{f_2\phi\phi}\Gamma^{(2)}_{\mu\nu\kappa\lambda}(p_3,p_4)F''^{(f_2\phi\phi)}(p_{34}^2),\end{aligned}\tag{3.32}$$

with $M_0=1$ GeV and dimensionless coupling constants $g'_{f_2\phi\phi}$ and $g''_{f_2\phi\phi}$ being free parameters. The explicit tensorial functions $\Gamma^{(i)}_{\mu\nu\kappa\lambda}(p_3,p_4)$, $i=0,2$, are given by (3.13) and (3.14), respectively. The relations (3.4) can now be checked from (3.27) and (3.32) using again (3.21) of [11]. Different form factors F' and F'' are allowed *a priori* in (3.32). We assume that

$$F'^{(f_2\phi\phi)}(p_{34}^2)=F''^{(f_2\phi\phi)}(p_{34}^2)=F^{(\mathbb{PP}f_2)}(p_{34}^2).\tag{3.33}$$

In the high-energy approximation, we can write the amplitude for the $\mathbb{PP}$ fusion as

$$\begin{aligned}\mathcal{M}^{(\mathbb{PP}\to f_2\to\phi\phi)\rho_3\rho_4}_{\lambda_a\lambda_b\to\lambda_1\lambda_2\phi\phi} &= 3\beta_{\mathbb{P}NN}2(p_1+p_a)_{\mu_1}(p_1+p_a)_{\nu_1}\delta_{\lambda_1\lambda_a}F_1(t_1)\frac{1}{4s_1}(-is_1\alpha'_{\mathbb{P}})^{\alpha_{\mathbb{P}}(t_1)-1}\\ &\times\Gamma^{(\mathbb{PP}f_2)\mu_1\nu_1,\mu_2\nu_2,\alpha\beta}(q_1,q_2)\Delta^{(f_2)}_{\alpha\beta,\kappa\lambda}(p_{34})\Gamma^{(f_2\phi\phi)\kappa\lambda\rho_3\rho_4}(p_3,p_4)\\ &\times\frac{1}{4s_2}(-is_2\alpha'_{\mathbb{P}})^{\alpha_{\mathbb{P}}(t_2)-1}3\beta_{\mathbb{P}NN}2(p_2+p_b)_{\mu_2}(p_2+p_b)_{\nu_2}\delta_{\lambda_2\lambda_b}F_1(t_2).\end{aligned}\tag{3.34}$$

We use in (3.34) the tensor-meson propagator with the simple Breit-Wigner form

$$\Delta^{(f_2)}_{\mu\nu,\kappa\lambda}(p_{34})=\frac{1}{p_{34}^2-m_{f_2}^2+im_{f_2}\Gamma_{f_2}}\left[\frac{1}{2}(\hat{g}_{\mu\kappa}\hat{g}_{\nu\lambda}+\hat{g}_{\mu\lambda}\hat{g}_{\nu\kappa})-\frac{1}{3}\hat{g}_{\mu\nu}\hat{g}_{\kappa\lambda}\right],\tag{3.35}$$

where $\hat{g}_{\mu\nu}=-g_{\mu\nu}+p_{34\mu}p_{34\nu}/p_{34}^2$, Γ_{f_2} is the total decay width of the f_2 resonance, and m_{f_2} is its mass. We take their numerical values from PDG [55]; see Table I in Sec. II.

C. Pseudoscalar and scalar resonance production

As was mentioned in Sec. I, the scalar $f_0(2100)$ and the pseudoscalar $\eta(2100)$, $\eta(2225)$, and $X(2500)$ states were seen in $J/\psi \to \gamma\phi\phi$ [43]. In [43] the authors found that the most significant contribution to $\phi\phi$ comes from the $\eta(2225)$ resonance.

The above resonances can also contribute to $\phi\phi$ CEP in addition to the continuum and the $f_2(2340)$ processes discussed in Secs. III A and III B, respectively. Therefore, in our analysis we should consider these possibilities. But for simplicity we will limit our discussion to the CEP of the $f_0(2100)$ and the $\eta(2225)$ mesons with subsequent decay to $\phi\phi$.

The Born amplitude for the $\mathbb{PP}$ fusion to $\phi\phi$ through an s-channel η-like resonance $\tilde{M}$ is given by

$$\begin{aligned}\mathcal{M}^{(\mathbb{PP}\to\tilde{M}\to\phi\phi)\rho_3\rho_4}_{\lambda_a\lambda_b\to\lambda_1\lambda_2\phi\phi} &= (-i)\bar{u}(p_1,\lambda_1)i\Gamma^{(\mathbb{P}pp)\mu_1\nu_1}(p_1,p_a)u(p_a,\lambda_a)i\Delta^{(\mathbb{P})}_{\mu_1\nu_1,\alpha_1\beta_1}(s_1,t_1)\\ &\times i\Gamma^{(\mathbb{PP}\tilde{M})\alpha_1\beta_1,\alpha_2\beta_2}(q_1,q_2)i\Delta^{(\tilde{M})}(p_{34})i\Gamma^{(\tilde{M}\phi\phi)\rho_3\rho_4}(p_3,p_4)\\ &\times i\Delta^{(\mathbb{P})}_{\alpha_2\beta_2,\mu_2\nu_2}(s_2,t_2)\bar{u}(p_2,\lambda_2)i\Gamma^{(\mathbb{P}pp)\mu_2\nu_2}(p_2,p_b)u(p_b,\lambda_b).\end{aligned} \tag{3.36}$$

The effective $\mathbb{PP}\tilde{M}$ vertex was discussed in Sec. 2.2 of [14]. As was shown there, in general more than one coupling structure $\mathbb{PP}\tilde{M}$ is possible. The general $\mathbb{PP}\tilde{M}$ vertex constructed in Sec. 2.2 of [14] corresponds to the sum of the values $(l,S)=(1,1)$ and (3,3) with the dimensionless coupling parameters $g'_{\mathbb{PP}\tilde{M}}$ and $g''_{\mathbb{PP}\tilde{M}}$, respectively. The resulting $\mathbb{PP}\tilde{M}$ vertex, including a form factor, is given as follows:

$$i\Gamma^{(\mathbb{PP}\tilde{M})}_{\mu\nu,\kappa\lambda}(q_1,q_2) = (i\Gamma^{\prime(\mathbb{PP}\tilde{M})}_{\mu\nu,\kappa\lambda}(q_1,q_2)|_{\rm bare} + i\Gamma^{\prime\prime(\mathbb{PP}\tilde{M})}_{\mu\nu,\kappa\lambda}(q_1,q_2)|_{\rm bare})\tilde{F}^{(\mathbb{PP}\tilde{M})}(q_1^2,q_2^2,p_{34}^2), \tag{3.37}$$

$$\begin{aligned}i\Gamma^{\prime(\mathbb{PP}\tilde{M})}_{\mu\nu,\kappa\lambda}(q_1,q_2)|_{\rm bare} &= i\frac{g'_{\mathbb{PP}\tilde{M}}}{2M_0}(g_{\mu\kappa}\varepsilon_{\nu\lambda\rho\sigma}+g_{\nu\kappa}\varepsilon_{\mu\lambda\rho\sigma}+g_{\mu\lambda}\varepsilon_{\nu\kappa\rho\sigma}+g_{\nu\lambda}\varepsilon_{\mu\kappa\rho\sigma})\\ &\times(q_1-q_2)^\rho p_{34}^\sigma,\end{aligned} \tag{3.38}$$

$$\begin{aligned}i\Gamma^{\prime\prime(\mathbb{PP}\tilde{M})}_{\mu\nu,\kappa\lambda}(q_1,q_2)|_{\rm bare} &= i\frac{g''_{\mathbb{PP}\tilde{M}}}{M_0^3}\{\varepsilon_{\nu\lambda\rho\sigma}[q_{1\kappa}q_{2\mu}-(q_1\cdot q_2)g_{\mu\kappa}]+\varepsilon_{\mu\lambda\rho\sigma}[q_{1\kappa}q_{2\nu}-(q_1\cdot q_2)g_{\nu\kappa}]\\ &+\varepsilon_{\nu\kappa\rho\sigma}[q_{1\lambda}q_{2\mu}-(q_1\cdot q_2)g_{\mu\lambda}]+\varepsilon_{\mu\kappa\rho\sigma}[q_{1\lambda}q_{2\nu}-(q_1\cdot q_2)g_{\nu\lambda}]\}\\ &\times(q_1-q_2)^\rho p_{34}^\sigma;\end{aligned} \tag{3.39}$$

see (2.4) and (2.6) of [14]. For $\tilde{M}=\eta$ and $\tilde{M}=\eta'(958)$, the corresponding coupling constants were fixed in [14] (see Table 4 there) to differential distributions of the WA102 Collaboration [25,28]. For the $\mathbb{PP}\eta(2225)$ coupling, relevant for CEP of $\phi\phi$, there are no data to determine it. Therefore, we consider, for simplicity, only the term $(l,S)=(1,1)$ in (3.37). That is, we set $g''_{\mathbb{PP}\eta(2225)}=0$. We take the same factorized form for the Pomeron-Pomeron-$\eta(2225)$ form factor as in (3.29)–(3.31).

For the $\eta\phi\phi$ vertex we make the following ansatz:

$$i\Gamma^{(\eta\phi\phi)}_{\mu\nu}(p_3,p_4) = i\frac{1}{2M_0}g_{\eta\phi\phi}\varepsilon_{\mu\nu\kappa\lambda}p_3^\kappa p_4^\lambda F^{(\eta\phi\phi)}(p_{34}^2), \tag{3.40}$$

with $M_0=1$ GeV and $g_{\eta\phi\phi}$ being a free parameter.

The amplitude for $\phi\phi$ CEP through the scalar $f_0(2100)$ meson is as for $\eta(2225)$ in (3.36) but with $\Gamma^{(\mathbb{PP}\eta)}$, $\Gamma^{(\eta\phi\phi)}$, and $\Delta^{(\eta)}$ replaced by $\Gamma^{(\mathbb{PP}f_0)}$, $\Gamma^{(f_0\phi\phi)}$, and $\Delta^{(f_0)}$, respectively. In Appendix A of [18], a similar amplitude for the reaction $pp\to pp(f_0\to\rho^0\rho^0)$ is written. The effective $\mathbb{PP}f_0$ vertex is discussed in detail in Appendix A of [14]. As was shown there, the $\mathbb{PP}f_0$ vertex corresponds to the sum of two (l,S) couplings, $(l,S)=(0,0)$ and (2,2), with corresponding coupling parameters $g'_{\mathbb{PP}f_0}$ and $g''_{\mathbb{PP}f_0}$, respectively. The vertex is written as follows:

$$\begin{aligned}i\Gamma^{(\mathbb{PP}f_0)}_{\mu\nu,\kappa\lambda}(q_1,q_2) &= (i\Gamma^{\prime(\mathbb{PP}f_0)}_{\mu\nu,\kappa\lambda}|_{\rm bare} + i\Gamma^{\prime\prime(\mathbb{PP}f_0)}_{\mu\nu,\kappa\lambda}(q_1,q_2)|_{\rm bare})\\ &\times\tilde{F}^{(\mathbb{PP}f_0)}(q_1^2,q_2^2,p_{34}^2);\end{aligned} \tag{3.41}$$

see (A.17)–(A.21) of [14]. Due to the same reason as for the $\eta(2225)$ meson, we restrict in (3.41) to one term $(l,S)=(0,0)$. We take the same form for the Pomeron-Pomeron-$f_0(2100)$ form factor as in (3.29)–(3.31).

In Appendix A of [18] we discussed our ansatz for the $f_0\rho\rho$ vertex; see (A.7) there. For the $f_0\phi\phi$ vertex, of interest to us here, we make the same ansatz but with coupling parameters $g'_{f_0\phi\phi}$ and $g''_{f_0\phi\phi}$ instead of $g'_{f_0\rho\rho}$ and

$g''_{f_0\rho\rho}$, respectively. For simplicity, we assume in the following $g'_{f_0\phi\phi}=0$. We get then

$$i\Gamma^{(f_0\phi\phi)}_{\mu\nu}(p_3,p_4)=i\frac{2}{M_0}g''_{f_0\phi\phi}[p_{4\mu}p_{3\nu}-(p_3\cdot p_4)g_{\mu\nu}]\times F''^{(f_0\phi\phi)}(p_{34}^2), \tag{3.42}$$

where $g''_{f_0\phi\phi}$ is a parameter to be determined from experiment. Here the $\mathbb{P}\mathbb{P}f_0(2100)$ and $f_0(2100)\phi\phi$ coupling parameters are essentially unknown at present.

A priori different form factors $F^{(\eta\phi\phi)}$ and $F''^{(f_0\phi\phi)}$ are allowed in (3.40) and (3.42), respectively. We assume $F^{(\eta\phi\phi)}=F''^{(f_0\phi\phi)}=F^{(\mathbb{P}\mathbb{P}f_2)}$; see Eq. (3.31).

D. Diffractive production of $\phi\phi$ continuum with Odderon exchanges

The diffractive production of two ϕ mesons seems to offer a good possibility to identify and/or study the Odderon exchanges [66]. At high energy there are two types of processes represented by the diagrams in Fig. 2. So far these processes have not yet been calculated or even estimated. A particularly important case worthy of attention is diagram (a) in Fig. 2. The advantage of this process compared to that in diagram (b) is that in diagram (a) no Odderon-proton vertex is involved. Because the coupling of the Odderon to the proton is probably small, one could expect $\sigma^{(\mathbb{O}-\mathbb{P}-\mathbb{O})}\ll\sigma^{(\mathbb{P}-\mathbb{O}-\mathbb{P})}$. Therefore, in the following we neglect the contribution with two Odderon exchanges in the calculation.

The amplitude for the process shown by diagram (a) in Fig. 2 has the same form as the amplitude with the ϕ-meson exchange discussed in Sec. III A; see Eqs. (3.6)–(3.8). But here we have to make the following replacements:

$$i\Delta^{(\phi)}_{\mu\nu}(\hat{p})\to i\Delta^{(\mathbb{O})}_{\mu\nu}(s_{34},\hat{p}^2), \tag{3.43}$$

$$i\Gamma^{(\mathbb{P}\phi\phi)}_{\mu\nu\kappa\lambda}(k',k)\to i\Gamma^{(\mathbb{P}\mathbb{O}\phi)}_{\mu\nu\kappa\lambda}(k',k). \tag{3.44}$$

Our ansatz for the effective propagator of the $C=-1$ Odderon follows (3.16) and (3.17) of [11],

$$i\Delta^{(\mathbb{O})}_{\mu\nu}(s,t)=-ig_{\mu\nu}\frac{\eta_{\mathbb{O}}}{M_0^2}(-is\alpha'_{\mathbb{O}})^{\alpha_{\mathbb{O}}(t)-1}, \tag{3.45}$$

$$\alpha_{\mathbb{O}}(t)=\alpha_{\mathbb{O}}(0)+\alpha'_{\mathbb{O}}t, \tag{3.46}$$

where in (3.45) we have $M_0^{-2}=1\ (\mathrm{GeV})^{-2}$ for dimensional reasons. Furthermore, $\eta_{\mathbb{O}}$ is a parameter with value ±1 and $\alpha_{\mathbb{O}}(t)$ is the Odderon trajectory, assumed to be linear in t. We choose, as an example, the slope parameter for the Odderon the same as for the Pomeron in (3.11). For the Odderon intercept we choose a number of representative values. That is, we shall show results for

$$\eta_{\mathbb{O}}=\pm1,\qquad \alpha'_{\mathbb{O}}=0.25\ \mathrm{GeV}^{-2},$$
$$\alpha_{\mathbb{O}}(0)=1.05,1.00,0.95. \tag{3.47}$$

The Odderon-exchange diagram presented in Fig. 2(a), due to the Regge-based parametrization with the Odderon intercept $\alpha_{\mathbb{O}}(0)\sim1.0$, should be especially relevant in the region of large rapidity separation of the ϕ mesons and large $\phi\phi$ invariant masses. This will be discussed further in Sec. IV C.

For the $\mathbb{P}\mathbb{O}\phi$ vertex we use an ansatz analogous to the $\mathbb{P}\rho\rho$ vertex; see (3.47) of [11]. We get then, orienting the momenta of the $\mathbb{O}$ and the ϕ outwards as shown in Fig. 3(a), the following formula:

$$i\Gamma^{(\mathbb{P}\mathbb{O}\phi)}_{\mu\nu\kappa\lambda}(k',k)=iF^{(\mathbb{P}\mathbb{O}\phi)}((k+k')^2,k'^2,k^2)\times[2a_{\mathbb{P}\mathbb{O}\phi}\Gamma^{(0)}_{\mu\nu\kappa\lambda}(k',k)-b_{\mathbb{P}\mathbb{O}\phi}\Gamma^{(2)}_{\mu\nu\kappa\lambda}(k',k)]. \tag{3.48}$$

Here k', μ and k, ν are the momentum and vector index of the Odderon and the ϕ, respectively; $a_{\mathbb{P}\mathbb{O}\phi}$ and $b_{\mathbb{P}\mathbb{O}\phi}$ are (unknown) coupling constants; and $F^{(\mathbb{P}\mathbb{O}\phi)}((k+k')^2,k'^2,k^2)$ is a form factor. In practical calculations we take the factorized form for the $\mathbb{P}\mathbb{O}\phi$ form factor,

$$F^{(\mathbb{P}\mathbb{O}\phi)}((k+k')^2,k'^2,k^2)=F((k+k')^2)F(k'^2)F^{(\mathbb{P}\mathbb{O}\phi)}(k^2), \tag{3.49}$$

where we adopt the monopole form

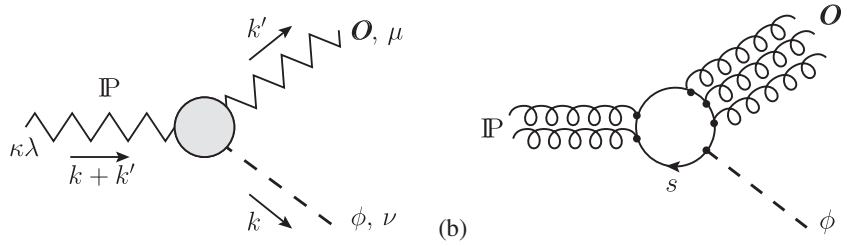

FIG. 3. (a) Generic diagram for the $\mathbb{P}\mathbb{O}\phi$ vertex with momentum and Lorentz-indices assignments. (b) A QCD diagram contributing to the $\mathbb{P}\mathbb{O}\phi$ vertex.

$$F(k^2) = \frac{1}{1 - k^2/\Lambda^2}, \tag{3.50}$$

and $F^{(\mathbb{P}\mathbb{O}\phi)}(k^2)$ is a form factor normalized to $F^{(\mathbb{P}\mathbb{O}\phi)}(m_\phi^2) = 1$. The coupling parameters $a_{\mathbb{P}\mathbb{O}\phi}$, $b_{\mathbb{P}\mathbb{O}\phi}$ in (3.48) and the cutoff parameter Λ^2 in the form factor (3.50) could be adjusted to experimental data.

In Fig. 3(b) we show a QCD diagram which will contribute to the $\mathbb{P}\mathbb{O}\phi$ vertex. The "normal" decay of a ϕ meson from the QCD point of view is to three gluons produced in the annihilation of the $s\bar{s}$ quarks. A higher order correction can involve a five-gluon decay. Turning such a diagram around we arrive at the $\mathbb{P}\mathbb{O}\phi$ coupling shown in Fig. 3(b).

For the considered reaction $pp \to pp\phi\phi$, the $\phi\phi$ subsystem energy $\sqrt{s_{34}} = M_{\phi\phi}$ is not very high and at threshold starts from $\sqrt{s_{34}} = 2m_\phi$. The Odderon-exchange amplitude applies for larger, certainly not too small, $\sqrt{s_{34}}$. At low energies the Regge type of interaction is not realistic and should be switched off. To achieve this requirement we shall multiply the Odderon-exchange amplitude by a simple, purely phenomenological factor:

$$F_{\rm thr}(s_{34}) = 1 - \exp\left(\frac{s_{\rm thr} - s_{34}}{s_{\rm thr}}\right), \tag{3.51}$$

with $s_{\rm thr} = 4m_\phi^2$. Our prescription leads to $\mathcal{M}^{(\mathbb{O}\text{-exchange})}_{pp\to pp\phi\phi} \to 0$ when $s_{34} \to s_{\rm thr}$. The form factors of Eqs. (3.49) and (3.50) then guarantee that in our calculation the Odderon only contributes in the Regge regime $|\hat{p}^2| \ll s_{34}$.

E. γ-exchange mechanism

The amplitude for the process shown by the diagram in Fig. 4 has the same form as the amplitude with the ϕ-meson exchange discussed in Sec. III A; see Eqs. (3.17) and (3.18). But we have to make the following replacements:

$$\Delta^{(\phi)}_{\rho_1\rho_2}(\hat{p}) \to \Delta^{(\gamma)}_{\rho_1\rho_2}(\hat{p}) = -\frac{g_{\rho_1\rho_2}}{\hat{p}^2}, \tag{3.52}$$

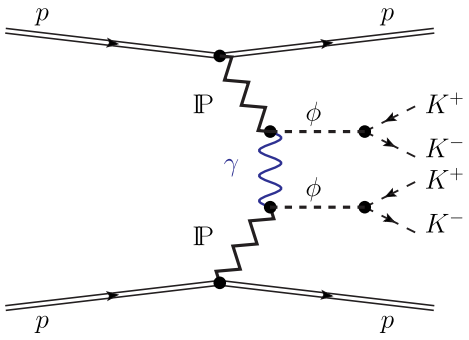

FIG. 4. The Born-level diagram for diffractive production of a ϕ-meson pair with an intermediate photon exchange.

$$\hat{F}_\phi(\hat{p}^2) \to \hat{F}_\gamma(\hat{p}^2), \tag{3.53}$$

where we assume that $\hat{F}_\gamma(\hat{p}^2) = F_M(\hat{p}^2)$ (3.16) and $\Lambda_0^2 = 1.0$ GeV^2, and

$$a_{\mathbb{P}\phi\phi} \to a_{\mathbb{P}\gamma\phi} = \frac{e}{\gamma_\phi} a_{\mathbb{P}\phi\phi}, \tag{3.54}$$

$$b_{\mathbb{P}\phi\phi} \to b_{\mathbb{P}\gamma\phi} = \frac{e}{\gamma_\phi} b_{\mathbb{P}\phi\phi}, \tag{3.55}$$

where $e > 0$, $\gamma_\phi < 0$, and $\gamma_\phi^2 = 4\pi/0.0716$ [see Eq. (5.3) of [61] and Eqs. (3.23)–(3.25) and Sec. 4 of [11]].

IV. RESULTS

In this section we wish to present first results for the $pp \to ppK^+K^-K^+K^-$ reaction via the intermediate $\phi(1020)\phi(1020)$ state corresponding to the diagrams shown in Figs. 1–4. In practice we work with the amplitudes in high-energy approximation; see (3.17) and (3.34).

A. Comparison with the WA102 data

It was noticed in [38] that the cross section for the production of a $\phi\phi$ system, for the same interval of $|x_{F,\phi\phi}| \le 0.2$, is almost independent of the center-of-mass energy. The experimental results are $\sigma^{(\phi\phi)}_{\rm exp} = 42 \pm 9$ nb at $\sqrt{s} = 12.7$ GeV [36], $\sigma^{(\phi\phi)}_{\rm exp} = 36 \pm 6$ nb at $\sqrt{s} = 23.8$ GeV [37], and $\sigma^{(\phi\phi)}_{\rm exp} = 41.0 \pm 3.7$ nb at $\sqrt{s} = 29.1$ GeV [38]. This suggests that the double-Pomeron-exchange mechanism shown in Fig. 1 is the dominant one for the $pp \to pp\phi\phi$ reaction in the above energy range. In the following we neglect, therefore, secondary Reggeon exchanges.

In principle, there are many possible resonances with $J^{PC} = 0^{++}$, 0^{-+}, 2^{++} that may contribute to the $pp \to pp\phi\phi$ reaction represented by the diagram (b) in Fig. 1; see the fifth column in Table I. Therefore, before comparing with the experimental data, let us first concentrate on the general characteristics of resonant production via the Pomeron-Pomeron fusion. We shall consider only three resonances as representative examples: $f_0(2100)$, $\eta(2225)$, and $f_2(2340)$. For illustration, in Fig. 5 we present the shape of distributions in $d{\rm P_t}$ and ϕ_{pp} for the experimental conditions as in the WA102 experiment [38], that is, for $\sqrt{s} = 29.1$ GeV and $|x_{F,\phi\phi}| \le 0.2$. Here $d{\rm P_t}$ is the "glueball-filter variable,"

$$\boldsymbol{dP_t} = \boldsymbol{q}_{t,1} - \boldsymbol{q}_{t,2} = \boldsymbol{p}_{t,2} - \boldsymbol{p}_{t,1}, \qquad d{\rm P_t} = |\boldsymbol{dP_t}|, \tag{4.1}$$

and ϕ_{pp} is the azimuthal angle between the transverse momentum vectors $\boldsymbol{p}_{t,1}$, $\boldsymbol{p}_{t,2}$ of the outgoing protons. The results without (the thin lines) and with (the thick lines) absorptive corrections are shown in Fig. 5. The differential

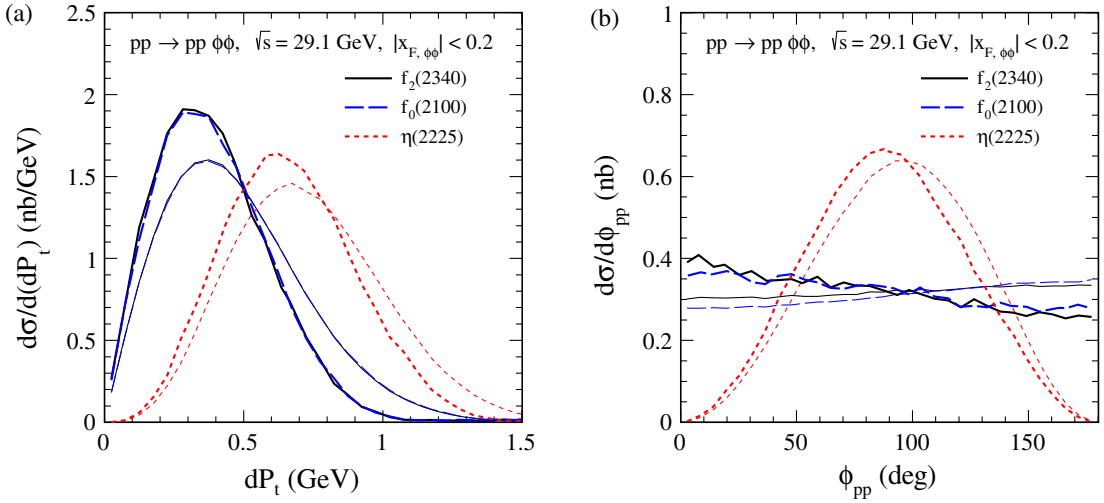

FIG. 5. The distribution in dP_t (4.1) and in ϕ_{pp} for the central exclusive $\phi\phi$ production at $\sqrt{s} = 29.1$ GeV and $|x_{F,\phi\phi}| \leq 0.2$. The results for scalar, pseudoscalar, and tensor resonances without (the thin lines) and with (the thick lines) absorptive corrections are shown. Because here we are interested only in the shape of the distributions, we normalized the differential distributions arbitrarily to 1 nb for both cases, with and without absorption corrections.

distributions have been normalized to 1 nb for both cases, with and without absorptive corrections. We can conclude that only the scalar and tensor resonances have similar characteristics as the WA102 experimental distributions [38] shown in Fig. 9 below. In the following we will assume that the $f_2(2340)$ resonance dominates.

In Fig. 6 we show the results for the $\phi\phi$ continuum process via the ϕ-meson exchange mechanism represented by diagram (a) in Fig. 1. In the left panel we present the $\phi\phi$ invariant mass distributions and in the right panel the distributions in $Y_{\text{diff}} = Y_3 - Y_4$. In our calculation we take $\Lambda_{\text{off},E} = 1.6$ GeV in (3.19) and the $\mathbb{P}\phi\phi$ coupling parameters from [20]. It is clearly seen from the left panel that the result without Reggeization (see the green solid line) is well above the WA102 experimental data [27,38] normalized to the total cross section $\sigma_{\text{exp}}^{(\phi\phi)} = 41$ nb from [38]. The Reggeization effect that leads to the suppression of the cross section should be applied here, but the way it should

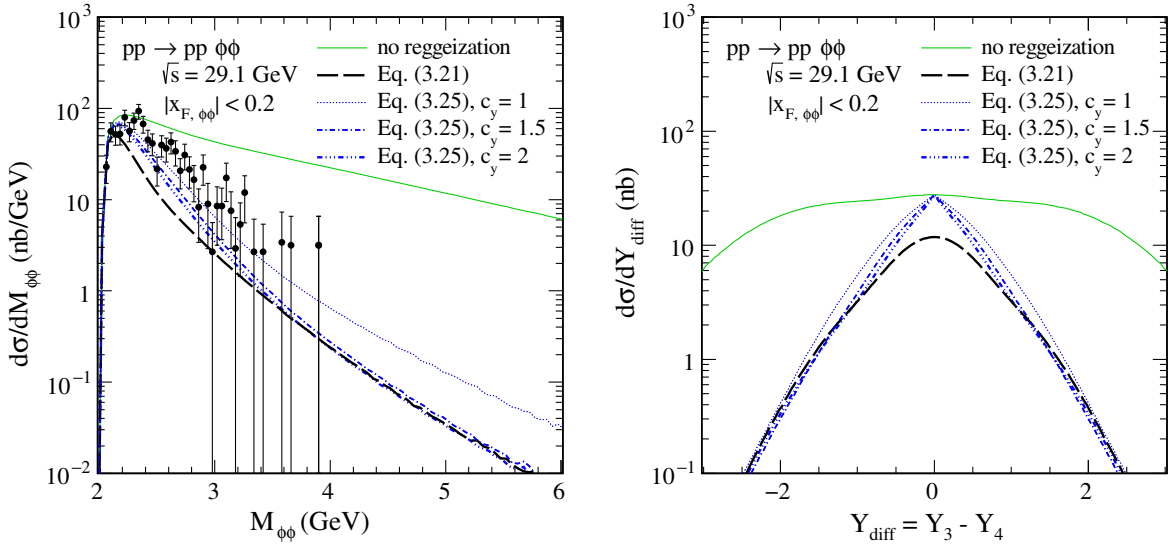

FIG. 6. The distributions in $\phi\phi$ invariant mass (the left panel) and in Y_{diff}, the rapidity distance between the two ϕ mesons (the right panel), for the ϕ-exchange continuum contribution. The calculations were done for $\sqrt{s} = 29.1$ GeV and $|x_{F,\phi\phi}| \leq 0.2$. In the left panel we show the WA102 experimental data [27] normalized to the total cross section $\sigma_{\text{exp}}^{(\phi\phi)} = 41$ nb from [38]. The green solid line corresponds to the non-Reggeized contribution. The results for the two prescriptions of Reggeization, (3.21) and (3.25), are shown by the black and blue lines, respectively. The absorption effects are included here.

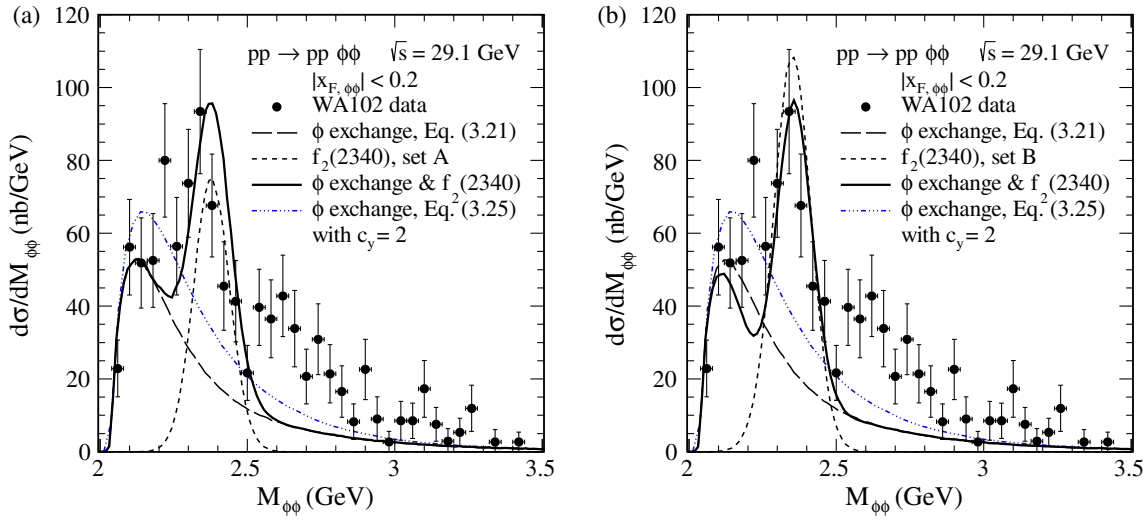

FIG. 7. Invariant mass distributions for the central $\phi\phi$ system compared to the WA102 data [27] at $\sqrt{s} = 29.1$ GeV and $|x_{F,\phi\phi}| \leq 0.2$. The data points have been normalized to the total cross section $\sigma_{\rm exp}^{(\phi\phi)} = 41$ nb from [38]. We show results for two sets of the parameters from Table II, set A [see panel (a)] and set B [see panel (b)]. The black long-dashed line corresponds to the Reggeized ϕ-exchange contribution [Eq. (3.21)], while the black short-dashed line corresponds to the $f_2(2340)$ resonance term, and the black solid line represents the coherent sum of both contributions. For comparison, we show also the blue dashed-dotted line that corresponds to the Reggeized ϕ-exchange contribution using Eq. (3.25). The absorption effects are included here.

be included is less obvious. We show results for two prescriptions of Reggeization given by Eqs. (3.21) and (3.25). We have checked that for the considered reaction $\langle -\hat{p}_t^2 \rangle$, $\langle -\hat{p}_u^2 \rangle \simeq 1$ GeV^2 (before Reggeization). We have $s_{34} - 4m_\phi^2 > 2$ GeV^2 for $\sqrt{s_{34}} = M_{\phi\phi} > 2.5$ GeV. It can therefore be expected that the prescription (3.21) is relevant near threshold and especially for $M_{\phi\phi} \lesssim 3$ GeV. However, in the light of the discussion after Eq. (3.21) how to treat the low-$M_{\phi\phi}$ region, we consider also the alternative prescription (3.25) combined with (3.26). In this case we present predictions for $c_y = 1$, 1.5, and 2 in (3.26). One can clearly see no effect of the Reggeization at $Y_{\rm diff} = 0$. The Reggeization becomes more important when $M_{\phi\phi}$ and $|Y_{\rm diff}|$ increase. For $c_y = 2$ and $M_{\phi\phi} \lesssim 3.5$ GeV we get similar results from (3.25) as from the first prescription (3.21).

In Fig. 7 we compare our predictions including now the two mechanisms shown in Fig. 1 to the WA102 data [27,38] for the $\phi\phi$ invariant mass distribution from the $pp \to pp\phi\phi$ reaction. With our choice to keep only one $\mathbb{P}\mathbb{P}f_2$ coupling from (3.28), namely, $g^{(1)}_{\mathbb{P}\mathbb{P}f_2}$, the distributions depend on the product of the couplings $g^{(1)}_{\mathbb{P}\mathbb{P}f_2} g'_{f_2\phi\phi}$ and $g^{(1)}_{\mathbb{P}\mathbb{P}f_2} g''_{f_2\phi\phi}$ with $g'_{f_2\phi\phi}$ and $g''_{f_2\phi\phi}$ given in (3.32). Again, for orientation purposes, we shall assume here and in the following that only either the first or the second of the above products of couplings is nonzero. In the parameter set A we choose $g^{(1)}_{\mathbb{P}\mathbb{P}f_2} g'_{f_2\phi\phi} \neq 0$, and in set B we choose $g^{(1)}_{\mathbb{P}\mathbb{P}f_2} g''_{f_2\phi\phi} \neq 0$; see Table II. Of course, once good measurements of all the relevant distributions of our reaction are available, one can try—as will be correct—to fit a linear combination of the above two coupling terms to the data. Thus, we show in Fig. 7 results for the two sets of parameters given in Table II, set A [see panel (a)] and set B [see panel (b)]. The long-dashed lines represent results for the Reggeized ϕ-exchange contribution. The short-dashed lines represent results for the $f_2(2340) \to \phi\phi$ resonance contribution. The solid lines represent the coherent sum of both contributions. We found a rather good agreement near $M_{\phi\phi} = 2.3$ GeV, taking into account only the continuum and $f_2(2340)$ meson, although the possibility of an $f_2(2300)$ meson contribution cannot be ruled out. Our predictions indicate therefore that in such a case we are dealing rather with an upper limit of the cross section for the f_2-resonance term. We wish to point out here that the interference of the continuum and resonance contributions depends on subtle details (choice of the couplings for resonant term, phase interpolation for the continuum term).

By comparing the theoretical results and the differential cross sections obtained by the WA102 Collaboration we fixed the parameters of the off-shell $\hat{t}/\hat{u}$-channel ϕ-meson form factor [$\Lambda_{{\rm off},E}$ in (3.19)] and the $\mathbb{P}\mathbb{P}f_2$ and $f_2\phi\phi$ couplings. For the convenience of the reader we have collected in Table II the default numerical values of the parameters of our model used in the calculations.

It can be observed that the WA102 experimental point at $M_{\phi\phi} \approx 2.2$ GeV is well above our theoretical result (ϕ-exchange contribution) and it may signal the presence of the $f_J(2220)$ resonance. As was shown in Fig. 5, mesons with $J = 0$ and $J = 2$ have similar characteristics. Therefore, the answer to the question about the spin of

TABLE II. Some parameters of our model. The columns indicate the equation numbers where the parameter is defined and their numerical values used in the calculations.

Parameters for ϕ-exchange mechanism	Equation	Value (Set A)	Value (Set B)
$a_{\mathbb{P}\phi\phi}$	(3.18); Sec. IV B of [20]	0.49 GeV^{-3}	0.49 GeV^{-3}
$b_{\mathbb{P}\phi\phi}$	(3.18); Sec. IV B of [20]	4.27 GeV^{-1}	4.27 GeV^{-1}
Λ_0^2	(3.16); Sec. IV B of [20]	1.0 GeV^2	1.0 GeV^2
$\Lambda_{\mathrm{off},E}$	(3.19)	1.6 GeV	1.6 GeV
$\mathbb{P}\mathbb{P} \to f_2(2340) \to \phi\phi$ mechanism			
$g^{(1)}_{\mathbb{P}\mathbb{P}f_2}\ g'_{f_2\phi\phi}$	(3.28) *et seq.*; (3.32)	12.0	0.0
$g^{(1)}_{\mathbb{P}\mathbb{P}f_2}\ g''_{f_2\phi\phi}$	(3.28) *et seq.*; (3.32)	0.0	7.0
$\tilde{\Lambda}_0^2$	(3.30)	1.0 GeV^2	1.0 GeV^2
Λ_{f_2}	(3.31)–(3.33)	1.0 GeV	1.0 GeV

$f_J(2220)$ cannot be easily given by studying the $\phi\phi$ decay channel. Our model calculation, including only two contributions, the Reggeized $\phi(1020)$-meson exchange and the production via the intermediate $f_2(2340)$, describes the WA102 experimental data up to $M_{\phi\phi} = 2.5$ GeV reasonably well; see Fig. 7. We cannot exclude a small contribution of the $X(2500)$ meson which was seen in $J/\psi \to \gamma\phi\phi$ [43]. Including the other resonances will only be meaningful once experiments with better statistics become available. Hopefully this will be the case at the LHC. The behavior at higher values of $M_{\phi\phi} \gtrsim 2.5$ GeV will be further discussed in Sec. IV C.

From Fig. 8 it is clearly seen that the shape of the Y_{diff} distribution is sensitive to the choice of the $f_2\phi\phi$ coupling (3.32) and of the Reggeization ansatz. For the ϕ continuum process we show the results obtained for the two Reggeization prescriptions, (3.21) and (3.25). Here Y_3, Y_4 are the rapidities of the two ϕ mesons. We show results in the $\phi\phi$ invariant mass window, $M_{\phi\phi} \in (2.2, 2.5)$ GeV, where tensor glueball candidates with masses around 2.3 GeV are expected. Two sets of the parameters, set A and set B, from Table II give different results. It can, therefore, be expected that the Y_{diff} variable will be very helpful in determining the $f_2\phi\phi$ coupling using results expected from LHC measurements, in particular, if they cover a wider range of rapidities. This will be presented further in Figs. 13 and 14. We have checked that for the reaction $pp \to pp(\mathbb{P}\mathbb{P} \to f_2(2340) \to \phi\phi)$ discussed here the shapes of the Y_{diff} distributions do not depend significantly on the choice of the $\mathbb{P}\mathbb{P}f_2$ vertex coupling (3.28). This is a different situation compared to the one observed by us for the $pp \to pp(\mathbb{P}\mathbb{P} \to f_2(1270) \to \pi^+\pi^-)$ reaction; see Figs. 7 and 8 of [4] and [21].

In Fig. 9 in the panels (a), (b), and (c) we compare our model results to the WA102 data on the differential distributions $d\sigma/d(\mathrm{dP_t})$, $d\sigma/d\phi_{pp}$, and $d\sigma/d|t|$ (that is,

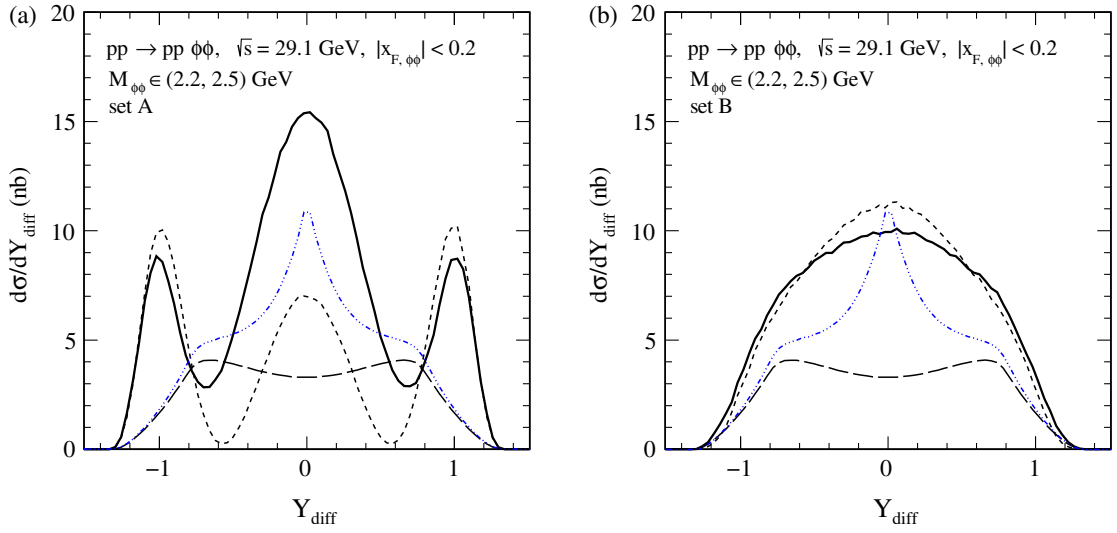

FIG. 8. The distributions in rapidity distance between two centrally produced $\phi(1020)$ mesons $Y_{\mathrm{diff}} = Y_3 - Y_4$ at $\sqrt{s} = 29.1$ GeV for $|x_{F,\phi\phi}| \le 0.2$ and $M_{\phi\phi} \in (2.2, 2.5)$ GeV. The meaning of the lines is the same as in Fig. 7. Here we show results for the two sets, A and B, of the parameters; see Table II. The absorption effects are included here.

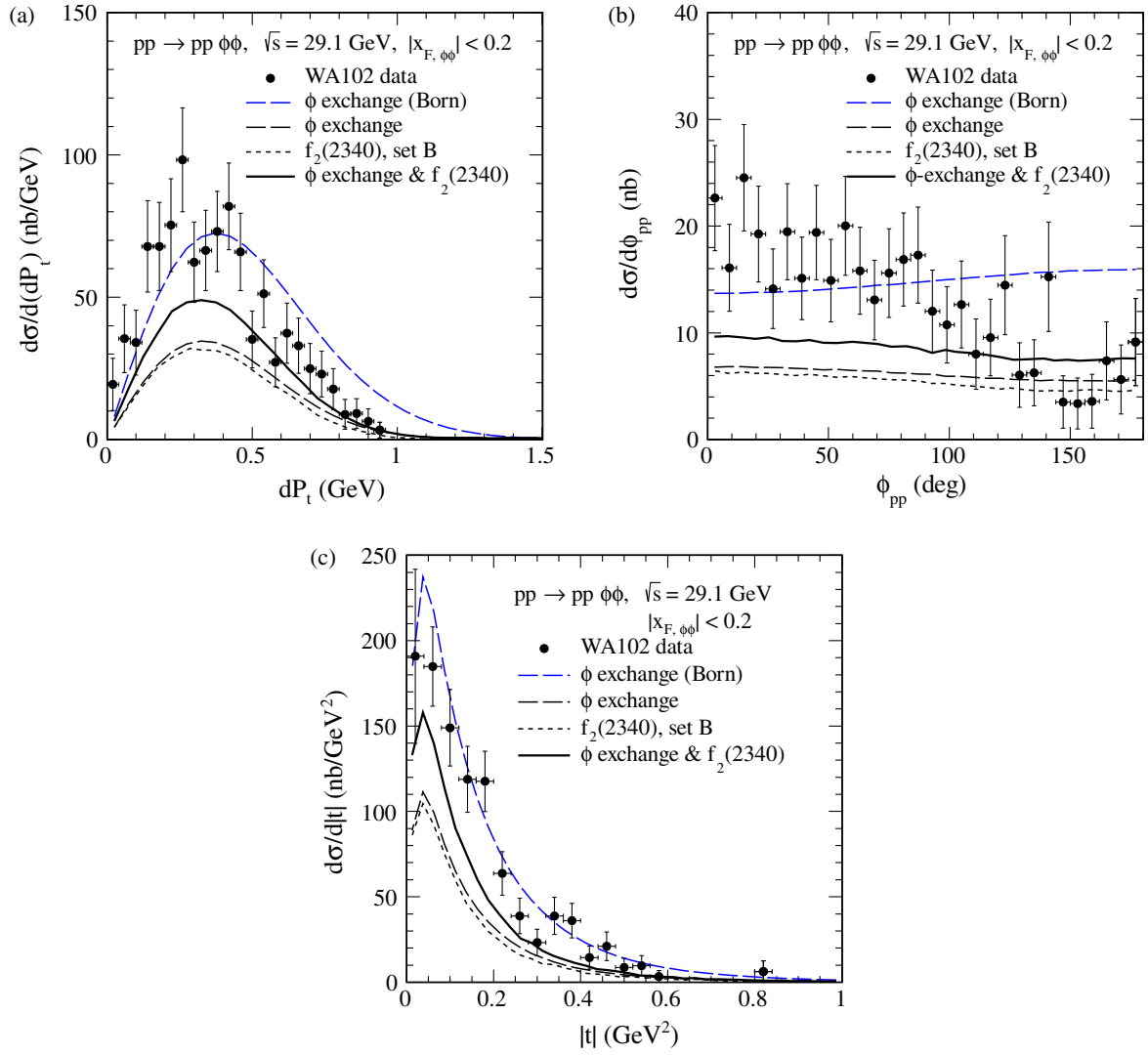

FIG. 9. Differential cross sections for the central exclusive $\phi\phi$ production at $\sqrt{s} = 29.1$ GeV and $|x_{F,\phi\phi}| \leq 0.2$. The data points from [38] have been normalized to the total cross section $\sigma_{\rm exp}^{(\phi\phi)} = 41$ nb given there. The meaning of the lines is the same as in Fig. 7(b) (set B). Here we show results for the ϕ-exchange contribution using Eq. (3.21). The absorption effects were included, but, for comparison, we also show the Reggeized ϕ-exchange contribution in the Born approximation (without absorption effects) corresponding to the upper blue long-dashed line.

$d\sigma/d|t_1|$ or $d\sigma/d|t_2|$), respectively. Here we used in the calculations the parameter set B of Table II. We have checked that for these three observables the results obtained with the parameter set A of Table II are similar. The theoretical results correspond to the calculations including absorptive effects calculated at the amplitude level and related to the pp nonperturbative interactions. Note that in the panels (a), (b), and (c) we also show the Born result for the ϕ-exchange contribution. The ratio of full and Born cross sections $\langle S^2 \rangle$ (the gap survival factor) at $\sqrt{s} = 29.1$ GeV is $\langle S^2 \rangle \cong 0.4$. From Figs. 5 and 9 we see the influence of absorption effects on the shape of distributions in ϕ_{pp} and dP_t.

So far we have tried to adjust parameters of the continuum and the $f_2(2340)$ resonance terms in order not to exceed the WA102 experimental data for the $\phi\phi$ invariant mass distribution. We see that limiting to these mechanisms we cannot describe the data for $M_{\phi\phi} > 2.5$ GeV. In consequence we underestimate experimental distributions also in Fig. 9. Clearly, an additional mechanism is needed to resolve this problem. We shall discuss a possible solution of this problem in Sec. IV C.

B. Predictions for the LHC experiments

We start from a discussion of the results for the $pp \to ppK^+K^-K^+K^-$ reaction obtained from the $\phi(1020)$-exchange mechanism discussed in Sec. III A. The calculations were done for $\sqrt{s} = 13$ TeV with typical experimental cuts on pseudorapidities and transverse

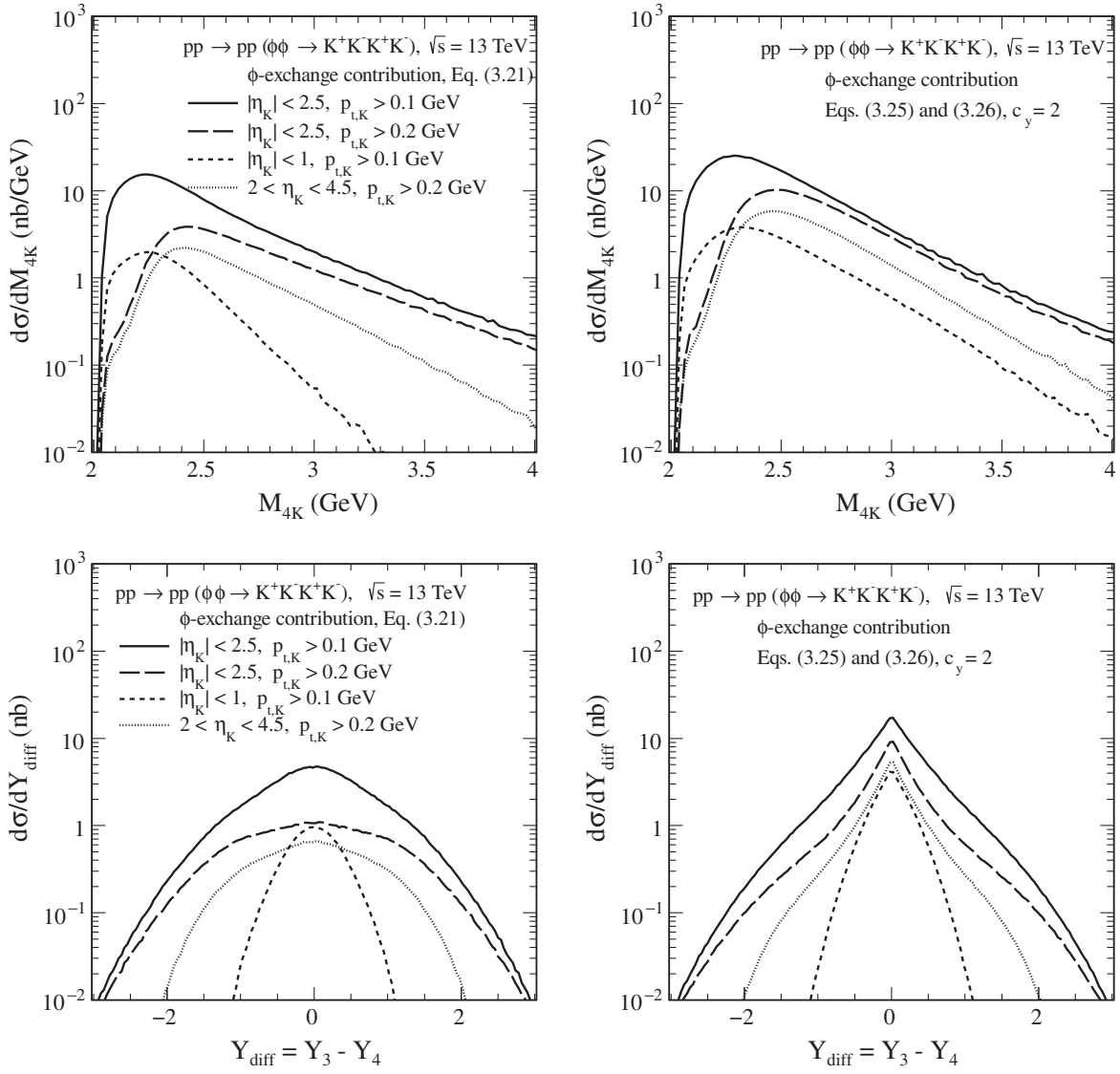

FIG. 10. Differential cross sections as a function of the four-kaon invariant mass (top panels) and as function of Y_{diff} (bottom panels) for the ϕ-exchange mechanism calculated for $\sqrt{s} = 13$ TeV with the kinematical cuts specified in the figure legends. The results for the two prescriptions of Reggeization (3.21) and (3.25) are presented. The absorption effects are included here.

momenta of centrally produced kaons. The ratio of the full and Born cross sections at $\sqrt{s} = 13$ TeV is approximately $\langle S^2 \rangle \cong 0.2$. In Fig. 10 we present the $K^+K^-K^+K^-$ invariant mass distributions (see the top panels) and the distributions in $Y_{\mathrm{diff}} = Y_3 - Y_4$ (see the bottom panels) calculated for $\sqrt{s} = 13$ TeV with the kinematical cuts specified in the figure legends. Here Y_3 and Y_4 mean $Y_{K^+K^-}$, where the kaons are produced from the same ϕ meson decay. Of course, the larger the detector coverage in η_K, the larger becomes $|Y_{\mathrm{diff}}|$. In the calculations we take into account the intermediate ϕ-meson Reggeization. We show results for the two prescriptions of Reggeization, (3.21) and (3.25); see the left and right panels, respectively. The results shown in the right panel were calculated with $c_y = 2$ in (3.26). We see that the choice of Reggeization has a large impact on the results. The Reggeization effect leads to a damping of the four-kaon invariant mass distributions. From the top panels, we see that increasing the $p_{t,K}$ cut from 0.1 to 0.2 GeV significantly suppresses the cross section at small M_{4K}. The first scenario of Reggeization, Eq. (3.21), also significantly suppresses the region when $Y_3 \approx Y_4$, that is, for $Y_{\mathrm{diff}} \simeq 0$. This is slightly different for the second Reggeization scenario (3.25); see the bottom right panel. The cross section for the $\phi\phi$-continuum contribution is about 2 orders of magnitude smaller than the cross section for the $\rho\rho$-continuum contribution discussed in [18].

In Fig. 11 we show further features of the M_{4K} and the Y_{diff} distributions for the ϕ-exchange contribution. We show results for the Reggeization prescription (3.21). The black solid line represents the complete result with the coherent sum of the $\hat{t}$- and $\hat{u}$-channel amplitudes; see Eqs. (3.7) and (3.8), respectively. The black long-dashed

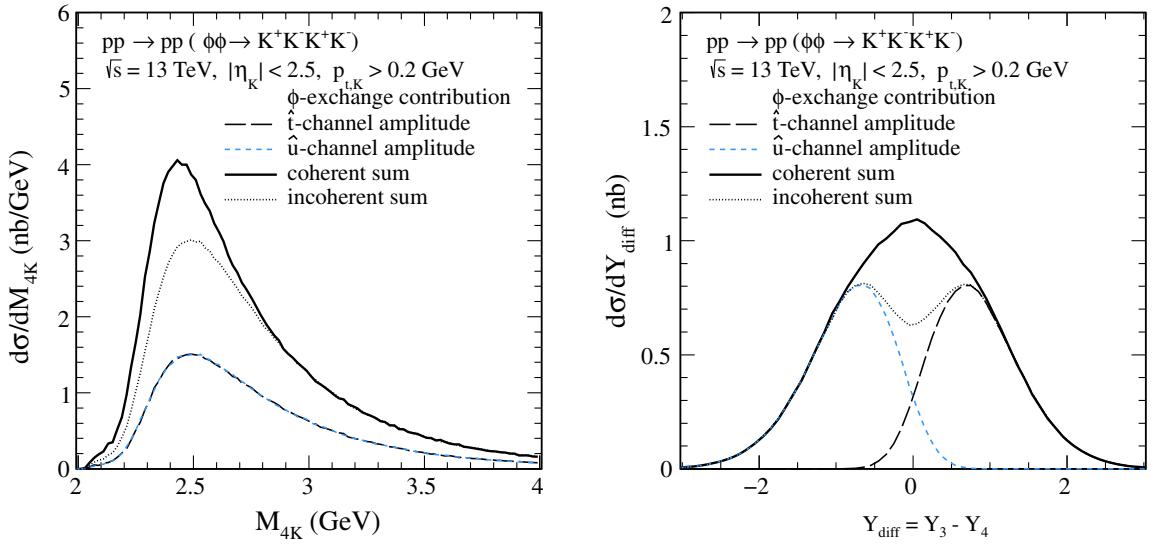

FIG. 11. Differential cross sections as a function of the four-kaon invariant mass (left panel) and as a function of $Y_{\rm diff}$ (right panel) for the $pp \to pp(\phi\phi \to K^+K^-K^+K^-)$ reaction calculated for $\sqrt{s} = 13$ TeV and $|\eta_K| < 2.5$, $p_{t,K} > 0.2$ GeV. The results for the ϕ-exchange contribution are presented. The black solid lines correspond to the coherent sum of the $\hat{t}$- and $\hat{u}$-channel amplitudes. Their incoherent sum is shown by the black dotted lines for comparison. The black long-dashed and blue short-dashed lines correspond to the results for the individual $\hat{t}$ and $\hat{u}$ terms, respectively. The absorption effects are included here.

and blue short-dashed lines represent the results for their individual contributions, respectively. The black dotted line corresponds to the incoherent sum of $\hat{t}$ and $\hat{u}$ contributions. We can see that the complete result indicates a large interference effect between the $\hat{t}$- and $\hat{u}$-channel diagrams. This effect occurs in the region at low M_{4K} and $|Y_{\rm diff}| < 1$. It can, therefore, be expected that the identification of diffractively produced high-mass resonances that decay into $\phi\phi$ pairs (e.g., η_c, χ_{c0}, χ_{c2}) should be possible at the LHC. For this purpose, one could study the distribution $d^2\sigma/dM_{4K}dY_{\rm diff}$ for the $pp \to ppK^+K^-K^+K^-$ reaction; see the discussion in [19] for the $pp \to ppp\bar{p}$ reaction.

In Fig. 12 we show the distribution in $(Y_{\rm diff}, M_{4K})$ for the continuum $4K$ production via the Reggeized ϕ-exchange mechanism. In the left panel we show the results for (3.21) and in the right panel for (3.25) and (3.26) with $c_y = 2$. We note that with our prescriptions of Reggeization and taking into account the kinematic cuts we have a clear correlation: large $|Y_{\rm diff}|$ automatically means large M_{4K}. Basically this is due to the fact that the transverse momenta of the

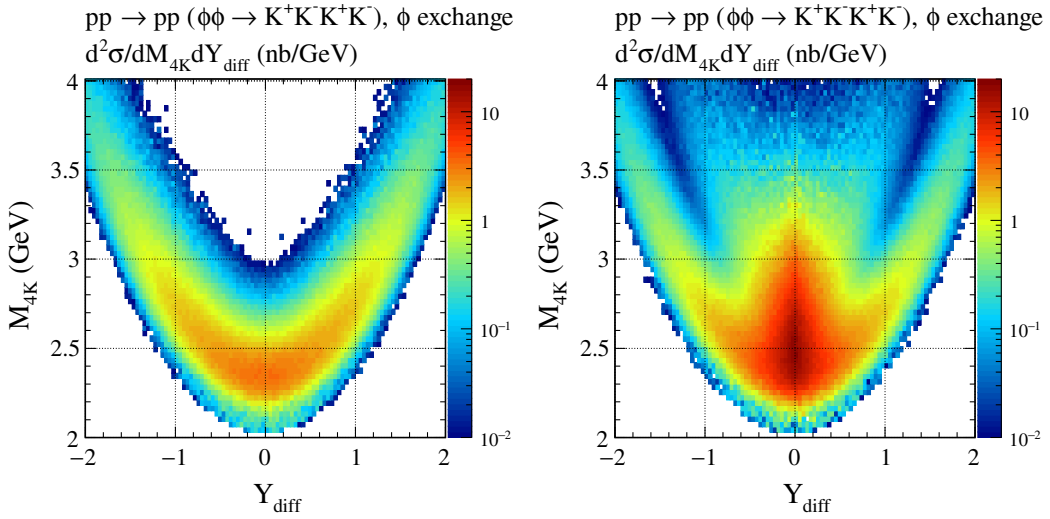

FIG. 12. The two-dimensional distributions in $(Y_{\rm diff}, M_{4K})$ for the diffractive continuum four-kaon production for $\sqrt{s} = 13$ TeV and $|\eta_K| < 2.5$, $p_{t,K} > 0.2$ GeV. The results for two prescriptions of Reggeization are presented. The result in the left panel corresponds to the prescription (3.21), and the result in the right panel corresponds to Eqs. (3.25) and (3.26) for $c_y = 2$. The absorption effects are included here.

outgoing ϕ mesons stay rather small due to the form factors in (3.17). The behavior of these distributions for large $M_{4K} = M_{\phi\phi}$ can be understood as follows. We are in essence studying here the reaction $\mathbb{P}\mathbb{P} \to \phi\phi$ through ϕ, respectively, for large $M_{\phi\phi}$ $\phi_{\mathbb{R}}$ (ϕ Reggeon) exchange. We expect then the maximum of this differential cross section for one ϕ forward and the other backward. This configuration corresponds to large M_{4K} and $|Y_{\mathrm{diff}}|$, giving the "ridge" in Fig. 12. In contrast, for M_{4K} near threshold the contributions from the $\hat{t}$ and $\hat{u}$ exchange diagrams overlap and interfere constructively; see Fig. 11. This effect gives the enhancement at small M_{4K} and small $|Y_{\mathrm{diff}}|$ in Fig. 12. Because of kinematic separation of the $\hat{t}$- and $\hat{u}$-channel continuum contributions for $M_{4K} > 3$ GeV the η_c and χ_c mesons could be searched for preferentially at $Y_{\mathrm{diff}} = 0$. If the Reggeization ansatz (3.21) is close to what is realized in nature these resonances η_c, χ_c should be clearly visible at small $|Y_{\mathrm{diff}}|$. However, the Reggeization ansatz (3.25) gives a larger continuum contribution at small $|Y_{\mathrm{diff}}|$; see also the lower panels of Fig. 10. Thus, if (3.25) is close to the truth, the identification of the above resonance contributions would be more difficult.

In Fig. 13 we present predictions for the $pp \to ppK^+K^-K^+K^-$ reaction including both the continuum ϕ-exchange contribution and the $f_2(2340)$ contribution for two sets of the parameters fixed from the WA102 data; see Fig. 7 and Table II. As can be clearly seen from Fig. 13, the resonance contribution generates, in both the M_{4K} and

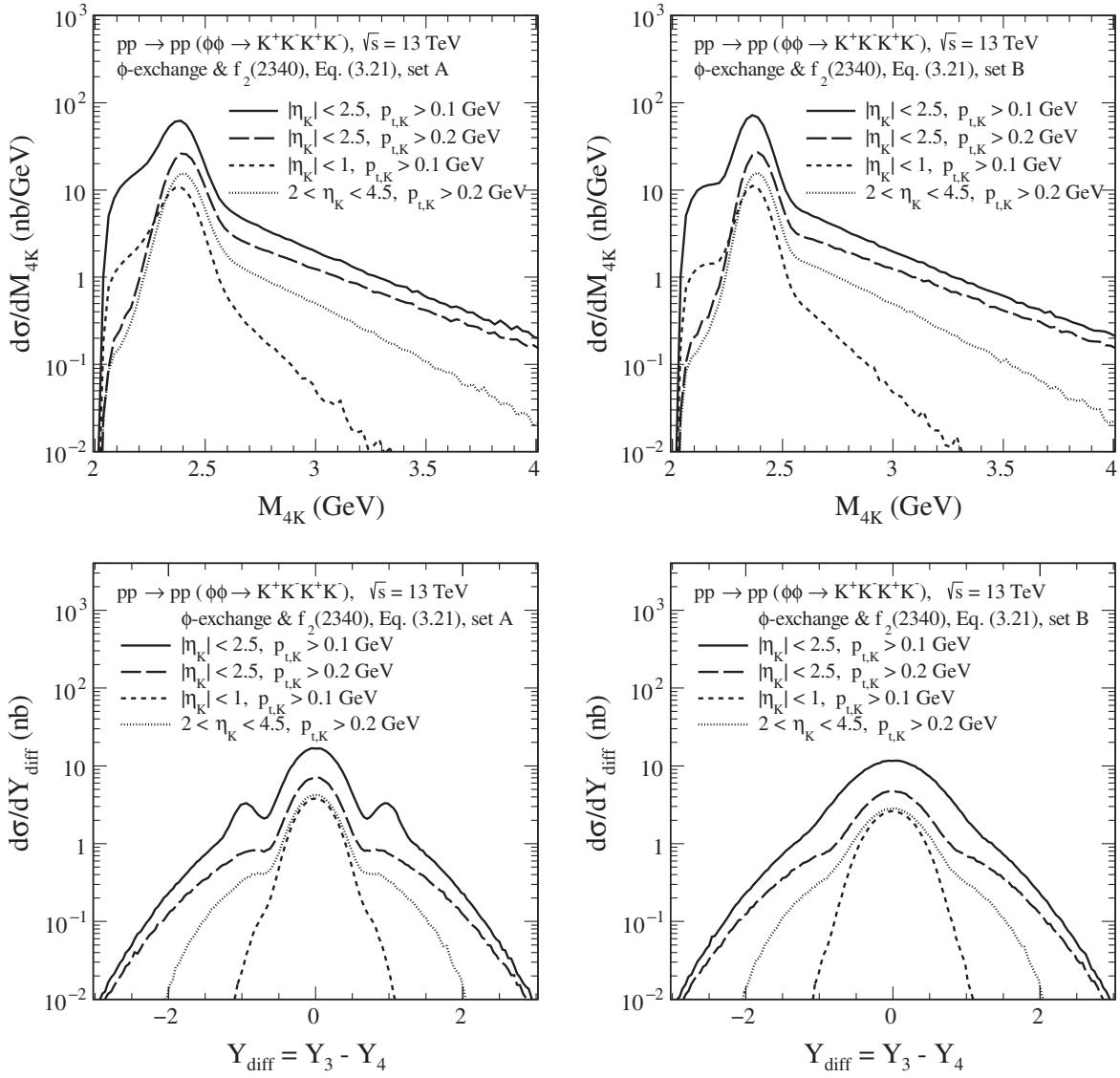

FIG. 13. Differential cross sections as a function of the four-kaon invariant mass (top panels) and as a function of Y_{diff} (bottom panels) at $\sqrt{s} = 13$ TeV for typical experimental cuts. The lines represent a coherent sum of the $\phi(1020)$-exchange and the $f_2(2340)$ terms. We show results for two sets of the parameters from Table II, set A (see the left panels) and set B (see the right panels). The absorption effects are included here.

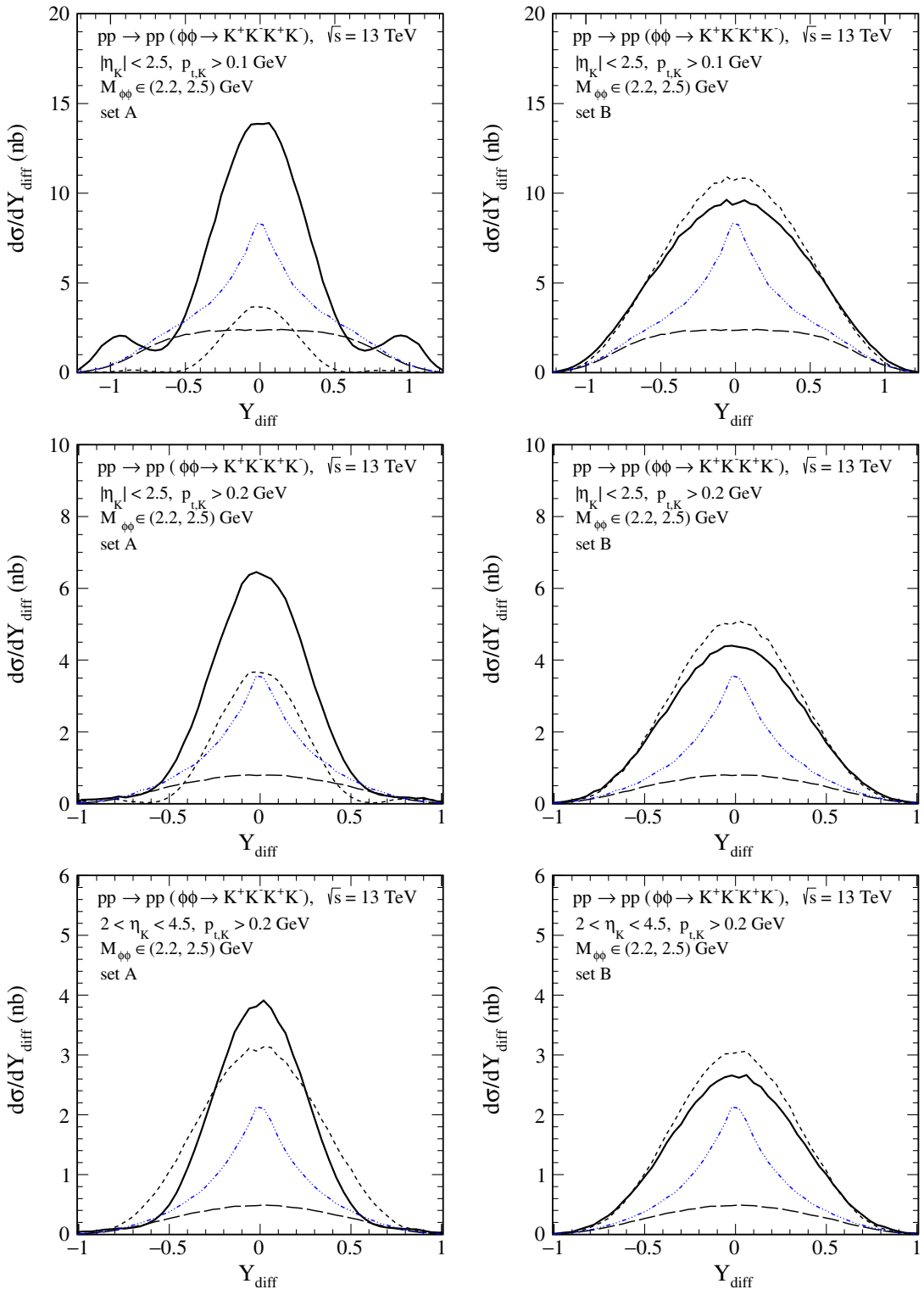

FIG. 14. The distributions in Y_{diff} at $\sqrt{s} = 13$ TeV for different experimental cuts on η_K and $p_{t,K}$, and for $M_{\phi\phi} \in (2.2, 2.5)$ GeV. The meaning of the lines is the same as in Fig. 7. The absorption effects are included here.

the Y_{diff} distributions, patterns with a complicated structure. In the calculations we include the ϕ-exchange contribution using the Reggeization prescription (3.21) and the dominant tensor $f_2(2340)$ resonance decaying into the $\phi\phi$ pair leading finally to the $K^+K^-K^+K^-$ final state. The resonance $f_2(2340)$ contribution is visible on top of the ϕ-exchange continuum contribution. We can see that the complete result indicates a large interference effect

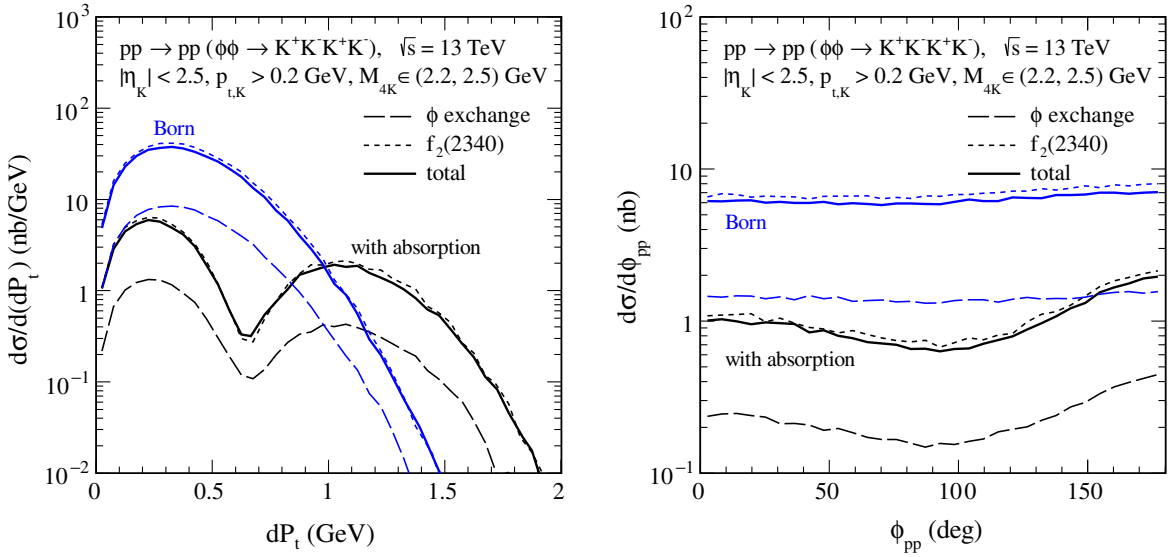

FIG. 15. Distributions in dP_t, the "glueball filter" variable (left panel), and in proton-proton relative azimuthal angle ϕ_{pp} (right panel) for the $pp \to pp(\phi\phi \to K^+K^-K^+K^-)$ reaction through the ϕ-exchange and $f_2(2340)$ mechanisms. Here the parameter set B from Table II and the Reggeization formula (3.21) were used. The predictions shown correspond to $\sqrt{s} = 13$ TeV and include cuts for $|\eta_K| < 2.5$, $p_{t,K} > 0.2$ GeV, and $M_{4K} \in (2.2, 2.5)$ GeV. The black lines correspond to the results with the absorption effects included. For comparison, the blue lines, marked "Born," correspond to the results without absorption.

of both terms. In principle, there may also be contributions from other tensor mesons and from η- and f_0-type mesons; see the fifth column in Table I.

In Fig. 14 we show the distributions in $Y_{\rm diff}$ for different experimental conditions, $|\eta_K| < 2.5$, $p_{t,K} > 0.2$ GeV, $|\eta_K| < 2.5$, $p_{t,K} > 0.1$ GeV, $2.0 < \eta_K < 4.5$, $p_{t,K} > 0.2$ GeV, from the top to bottom panels, respectively, and in the mass range $M_{\phi\phi} \in (2.2, 2.5)$ GeV. We show results for the two sets, A and B, of the parameters corresponding to the left and right panels. For the ϕ-exchange contribution we show also results for the alternative prescription (3.25) and for $c_y = 2$ in (3.26). From Figs. 13 (bottom panels) and 14 we can see that the distribution in $Y_{\rm diff}$ can be used to determine the $f_2(2340) \to \phi\phi$ coupling (3.32), in particular, if low $p_{t,K}$ will be available.

In Fig. 15 we discuss the observables dP_t (4.1) and ϕ_{pp} for which the distributions are very sensitive to the absorption effects. The results shown correspond to $\sqrt{s} = 13$ TeV and include cuts for $|\eta_K| < 2.5$, $p_{t,K} > 0.2$ GeV, and $M_{4K} \in (2.2, 2.5)$ GeV. Quite a different pattern can be seen for the Born case and for the case with absorption included. The absorptive corrections lead to significant modification of the shape of the ϕ_{pp} distribution and lead to an increase of the cross section for large dP_t. This effect could be verified in future experiments when both protons are measured, e.g., by the CMS-TOTEM and the ATLAS-ALFA experimental groups.

In Table III we have collected integrated cross sections in nb for different experimental cuts for the exclusive $K^+K^-K^+K^-$ production, including only the contributions shown in Fig. 1. The results were obtained in the calculations with the tensor Pomeron exchanges. The absorption effects were included in the calculations.

TABLE III. The integrated cross sections in nb for the central exclusive $K^+K^-K^+K^-$ production in proton-proton collisions via the intermediate $\phi\phi$ system due to the mechanisms shown in Fig. 1. The results have been calculated for $\sqrt{s} = 13$ TeV and some typical experimental cuts using the parameter set B from Table II. The calculations for the ϕ-exchange contribution were made using (3.21). The absorption effects are included here.

		Cross sections (nb)		
$\sqrt{s}$ (TeV)	Cuts	Total	ϕ exchange	$f_2(2340)$
13	$\lvert\eta_K\rvert < 1$, $p_{t,K} > 0.1$ GeV	2.11	0.83	2.00
13	$\lvert\eta_K\rvert < 2.5$, $p_{t,K} > 0.1$ GeV	16.16	8.30	12.80
13	$\lvert\eta_K\rvert < 2.5$, $p_{t,K} > 0.2$ GeV	5.75	2.67	4.47
13	$2 < \eta_K < 4.5$, $p_{t,K} > 0.2$ GeV	3.06	1.26	2.62

C. Results including Odderon exchange

In this section we shall discuss possibilities to observe Odderon-exchange effects in the CEP of $\phi\phi$ pairs.

The Odderon was introduced on theoretical grounds in [67,68]. For a review of the Odderon, see, e.g., [66]. Recent experimental results by the TOTEM Collaboration [69,70] have brought the Odderon question to the forefront again. For recent theoretical papers dealing with the Odderon, see, e.g., [11,15], which came out before the TOTEM results, and [71–77].

Clearly, it is of great importance in this context to study possible Odderon effects in reactions other than proton-proton elastic scattering. We shall argue here that the CEP of a $\phi\phi$ state offers a very nice way to look for Odderon effects as suggested in [66].

In Figs. 16 and 17 we show results for the diffractive CEP of $\phi\phi$ pairs including the mechanism with Odderon exchange shown in Fig. 2(a). Here we take the following values of the parameters for the Odderon exchange:

$$\eta_{\mathbb{O}} = \pm 1, \qquad \alpha_{\mathbb{O}}(0) = 1.05, \qquad a_{\mathbb{PO}\phi} = 0,$$
$$b_{\mathbb{PO}\phi} = 1.0, 1.5 \text{ GeV}^{-1}; \tag{4.2}$$

see (3.47), (3.48), and $\Lambda^2 = 1.0$ GeV^2 in (3.50). In the calculations we have used the parameter set B of Table II for the $\mathbb{PP}f_2$ contribution. For the case of ϕ exchange we have used the formula of Reggeization (3.21). In Fig. 16 we show the results for $\sqrt{s} = 29.1$ GeV and compare them to the WA102 data. Figure 17 shows the predictions for $\sqrt{s} = 13$ TeV using the same parameters. We show the ϕ-meson-exchange contribution (see the black long-dashed line), the $f_2(2340)$ contribution (see the black dashed line), and the Odderon-exchange contribution (see the red dotted line). The black dotted-dashed line corresponds to the photon-exchange contribution, represented by the diagram in Fig. 4, multiplied by a factor 10^3 to be visible in the figure. The coherent sum of all contributions is shown by the red and blue solid lines, corresponding to $\eta_{\mathbb{O}} = -1$ and $\eta_{\mathbb{O}} = +1$, respectively. Clearly, the complete result indicates a large interference effect between the ϕ- and Odderon-exchange diagrams. We see from the right panel of Fig. 16 that for $M_{\phi\phi} \gtrsim 2.5$ GeV the WA102 data leave room for a possible Odderon contribution which here we normalized in such a way as not to exceed the WA102 cross section. Such an Odderon contribution with $b_{\mathbb{PO}\phi} = 1.5$ GeV^{-1} can be treated then rather as an upper limit. Of course the "true" Odderon contribution may be much smaller.

In Fig. 17 we show the results for the ATLAS experimental conditions ($|\eta_K| < 2.5$, $p_{t,K} > 0.2$ GeV). For the Odderon term we take here again the parameters (4.2). With these the Odderon term gives a large enhancement of the M_{4K} distribution for $M_{4K} \gtrsim 3$ GeV and clearly dominates at large $|Y_{\text{diff}}|$. Whereas for $M_{4K} \gtrsim 3$ GeV and $\eta_{\mathbb{O}} = +1$ there is constructive interference of the ϕ-exchange and the Odderon terms, for $\eta_{\mathbb{O}} = -1$ the interference is destructive.

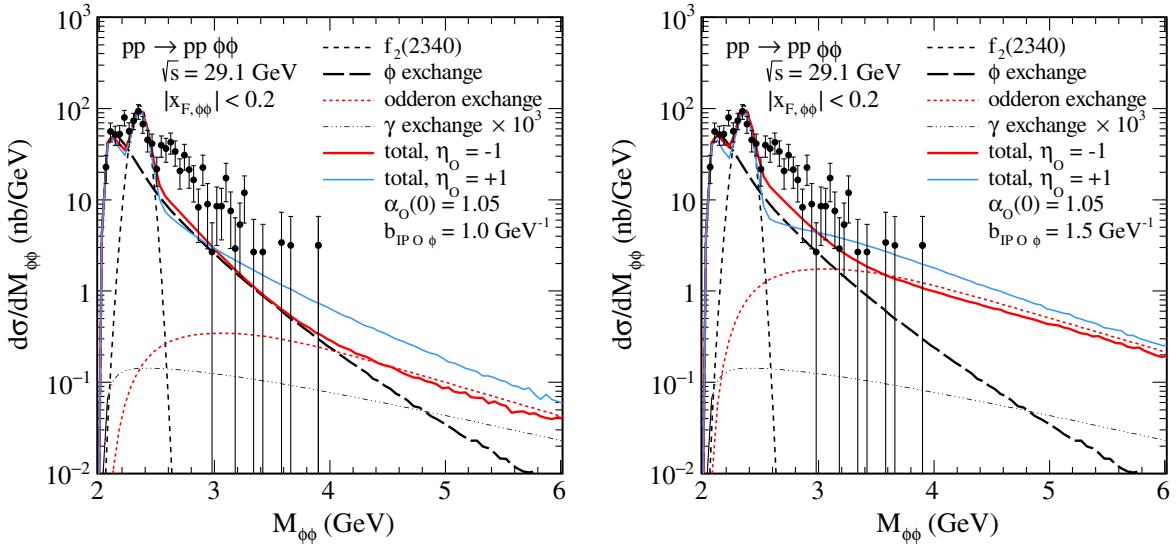

FIG. 16. Invariant mass distributions for the central production of $\phi\phi$ at $\sqrt{s} = 29.1$ GeV and $|x_{F,\phi\phi}| \leq 0.2$ together with the WA102 data [38] are shown. The black long-dashed line corresponds to the ϕ-exchange contribution and the black dashed line corresponds to the $f_2(2340)$ contribution. The black dotted-dashed line corresponds to the γ-exchange contribution enlarged by a factor 10^3. In the calculations the parameter set B of Table II for the ϕ-exchange and f_2 terms and the parameters (4.2) for the Odderon term have been used. The red dotted line represents the Odderon-exchange contribution for $a_{\mathbb{PO}\phi} = 0$, $b_{\mathbb{PO}\phi} = 1.0$ GeV^{-1} (left panel) and for $a_{\mathbb{PO}\phi} = 0$, $b_{\mathbb{PO}\phi} = 1.5$ GeV^{-1} (right panel). The coherent sum of all terms is shown by the red and blue solid lines for $\eta_{\mathbb{O}} = -1$ and $\eta_{\mathbb{O}} = +1$, respectively. Here we take $\alpha_{\mathbb{O}}(0) = 1.05$. The absorption effects are included in the calculations.

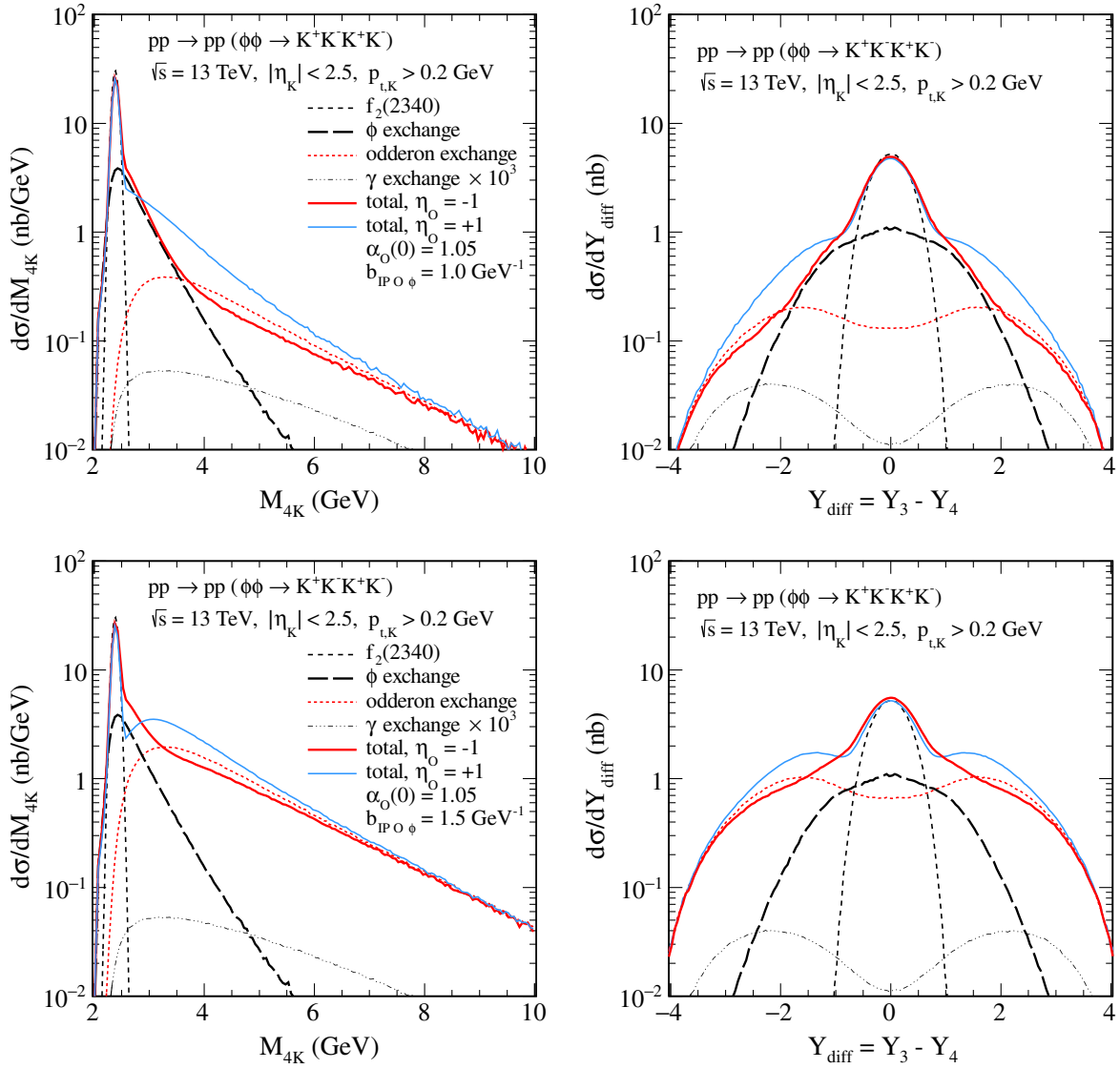

FIG. 17. The distributions in M_{4K} (left panels) and in Y_{diff} (right panels) for the $pp \to pp(\phi\phi \to K^+K^-K^+K^-)$ reaction calculated for $\sqrt{s} = 13$ TeV and $|\eta_K| < 2.5$, $p_{t,K} > 0.2$ GeV. The meaning of the lines is the same as in Fig. 16. The red and blue solid lines correspond to the complete results with $\eta_{\mathbb{O}} = -1$ and $\eta_{\mathbb{O}} = +1$, respectively. The results for $b_{\mathbb{P}\mathbb{O}\phi} = 1.0$ GeV^{-1} (top panels) and for $b_{\mathbb{P}\mathbb{O}\phi} = 1.5$ GeV^{-1} (bottom panels) are presented. The absorption effects are included in the calculations.

But in any case, for $M_{4K} \gtrsim 4$ GeV and $|Y_{\mathrm{diff}}| \gtrsim 2$ the Odderon term wins.

In Fig. 18 we show the complete result including the Odderon exchange with $\eta_{\mathbb{O}} = -1$ and various values of the Odderon intercept $\alpha_{\mathbb{O}}(0)$:

$$\eta_{\mathbb{O}} = -1, \qquad \alpha_{\mathbb{O}}(0) = 0.95, 1.00, 1.05. \tag{4.3}$$

Even a much smaller Odderon contribution should be visible for $M_{4K} \gtrsim 5$ GeV and $|Y_{\mathrm{diff}}| > 3$, provided the experimental statistics (luminosity) is sufficient. The distributions in M_{4K} and Y_{diff} seem therefore to offer good ways to identify the Odderon exchange if it is there.

The small intercept of the ϕ Reggeon exchange, $\alpha_\phi(0) = 0.1$ [64], makes the ϕ-exchange contribution steeply falling with increasing M_{4K} and $|Y_{\mathrm{diff}}|$. Therefore, an Odderon with an intercept $\alpha_{\mathbb{O}}(0)$ around 1.0 should be clearly visible in these distributions if the $\mathbb{P}\mathbb{O}\phi$ coupling is of reasonable size. This is, at least, the conclusion of our present model study. Of course, in a real experiment many investigations of the background will be necessary before one could claim to have seen Odderon exchange. Sources of background are $\phi_{\mathbb{R}}$ Reggeon exchange as discussed in the present paper. But one will also have to consider $\omega_{\mathbb{R}}$ Reggeon exchange and double ϕ production from two independent exchanges as shown in Fig. 19.

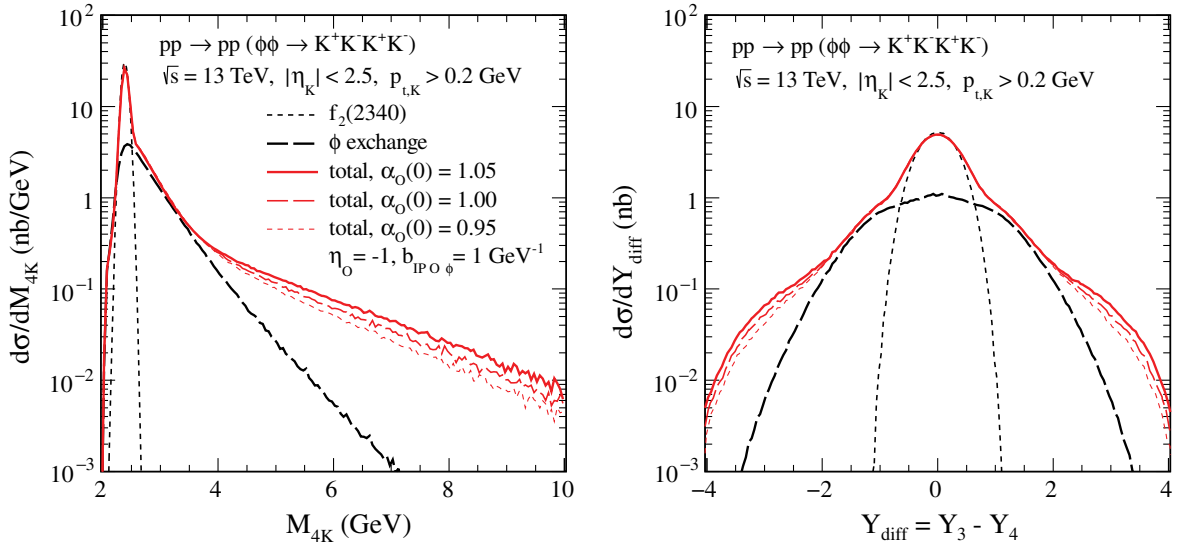

FIG. 18. The complete results for $\sqrt{s} = 13$ TeV and $|\eta_K| < 2.5$, $p_{t,K} > 0.2$ GeV are shown. Here we show results for $\eta_{\mathbb{O}} = -1$, $a_{\mathbb{PO}\phi} = 0$, $b_{\mathbb{PO}\phi} = 1$ GeV^{-1}, and for various values of the Odderon intercept $\alpha_{\mathbb{O}}(0)$.

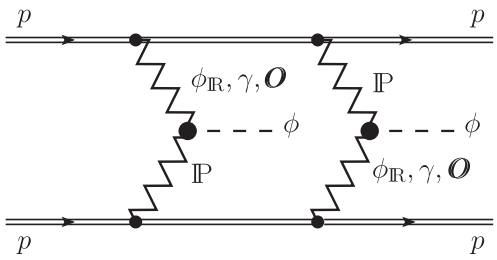

FIG. 19. Example of a diagram for the production of two ϕ mesons by two independent exchanges.

V. CONCLUSIONS

In the present paper we have presented first estimates of the contributions to the reaction $pp \to ppK^+K^-K^+K^-$ via the intermediate $\phi(1020)\phi(1020)$ resonance pairs. This reaction is being analyzed experimentally by the ALICE, ATLAS, CMS, and LHCb collaborations. The analysis of the reaction $pp \to pp(\mathbb{PP} \to f_2 \to \phi\phi)$ can be used for an identification of the tensor meson states. We note that the states $f_2(2300)$ and $f_2(2340)$ are good candidates for tensor glueballs.

We have considered the Pomeron-Pomeron fusion to $\phi\phi$ through the continuum process, with the $\hat{t}$- and $\hat{u}$-channel ϕ-meson exchange, and through the s-channel resonance reaction $[\mathbb{PP} \to f_2(2340) \to \phi\phi]$. The amplitudes for the process have been obtained within the tensor-Pomeron approach [11]. By comparing our theoretical results to the cross sections found by the WA102 Collaboration [27,38], we have fixed some coupling parameters and the off-shell dependencies of the intermediate ϕ mesons. We have discussed also the $\phi\phi$ production through the $f_0(2100)$ and $\eta(2225)$ resonances, which were observed in radiative decays of J/ψ [43]. We have shown that the contribution of the pseudoscalar $\eta(2225)$ meson is disfavored by the WA102 experimental distributions.

We have made estimates of the integrated cross sections as well as shown several differential distributions for different experimental conditions. The distribution in Y_{diff}, the rapidity difference between the two ϕ-mesons, depends strongly on the choice of the $f_2(2340) \to \phi\phi$ coupling. The general $f_2\phi\phi$ coupling is a sum of two basic couplings multiplied with two coupling constants; see (3.32). Our default values of the coupling parameters in the $\mathbb{PP}f_2$ and $f_2\phi\phi$ vertices can be verified by future experimental results to be obtained at the LHC. Future studies at the LHC could potentially determine them separately. Low-$p_{t,K}$ cuts are required for this purpose. It has been shown that absorption effects change considerably the shapes of the "glueball-filter variable" distributions as well as those for the azimuthal angle between the outgoing protons.

The study of the $pp \to pp\phi\phi$ reaction offers the possibility to search for effects of the Odderon. Such double diffractive production of two vector mesons with Odderon exchange as a means to look for the latter was discussed in [66]. In the present paper we have presented a concrete calculation of this process. Odderon contributions in diffractive production of single vector mesons, e.g., $pp \to pp\phi$, were investigated in [78]. In the diffractive production of ϕ meson pairs, it is possible to have Pomeron-Pomeron fusion with intermediate $\hat{t}/\hat{u}$-channel $C = -1$ Odderon exchange. The presence of Odderon exchange in the middle of the diagram should be important and distinguishable from other contributions for relatively large rapidity separation between the ϕ mesons. Hence, to study this type of mechanism one should investigate

events with rather large four-kaon invariant masses, outside of the region of resonances. These events are then "three-gap events": proton–gap–ϕ–gap–ϕ–gap–proton. Experimentally, this should be a clear signature. A study of such events should allow a determination of the Pomeron-Odderon-ϕ meson coupling, or at least of an upper limit for it. Of course, one will have to investigate in detail the contribution of other exchanges like the $\phi_{\mathbb{R}}$ Reggeon exchange studied in the present work. This could be done, for instance, by adjusting couplings and form factors at lower $M_{\phi\phi}$ and then studying the extrapolations to higher $M_{\phi\phi}$ where $\phi_{\mathbb{R}}$ exchange is a "background" to Odderon exchange. Experimentally one has to make sure that one is really dealing with three-gap events. Thus, additional meson production in the gaps, a reducible background, must be excluded. There is, however, also the irreducible background from the production of two ϕ mesons by two independent exchanges; see Fig. 19. This has to be estimated theoretically and, in a sense, is an absorptive correction. If an Odderon exchange is seen, then the distributions of the four-kaon invariant mass and of the rapidity difference between the two ϕ mesons will reveal the intercept of the Odderon trajectory.

In conclusion we note the following. If the final protons in our reaction (3.1) can be measured, one can reconstruct the complete kinematics of the reaction $\mathbb{P}+\mathbb{P}\to\phi+\phi$. A detailed study of this reaction as a function of its c.m. energy $M_{\phi\phi}$ and its momentum transfer should then be possible. The great caveat is that one has to get the absorption corrections under good theoretical control. The resonances at low $M_{\phi\phi}$ could then be investigated in detail. The special feature of the above reaction, however, is that the leading term at high energies must be due to a charge conjugation $C=-1$ exchange since $C=+1$ exchanges like the Pomeron cannot contribute. Therefore, an Odderon would give the leading term if its intercept is higher than that of the normal $C=-1$ Reggeons. Clearly, an experimental study of CEP of a ϕ-meson pair should be very valuable for clarifying the status of the Odderon. Finally we note that analogous reactions which are suitable for Odderon studies (see [66]) are double J/ψ and double Υ central exclusive production.

ACKNOWLEDGMENTS

We are indebted to Carlo Ewerz for discussions and comments. This research was partially supported by the Polish National Science Centre Grant No. 2014/15/B/ST2/02528 and by the Center for Innovation and Transfer of Natural Sciences and Engineering Knowledge, Republic of Poland/PL in Rzeszów.

[1] K. Akiba *et al.* (LHC Forward Physics Working Group), LHC forward physics, J. Phys. G **43**, 110201 (2016).
[2] T. A. Aaltonen *et al.* (CDF Collaboration), Measurement of central exclusive $\pi^+\pi^-$ production in $p\bar{p}$ collisions at $\sqrt{s}=0.9$ and 1.96 TeV at CDF, Phys. Rev. D **91**, 091101 (2015).
[3] V. Khachatryan *et al.* (CMS Collaboration), Exclusive and semi-exclusive $\pi^+\pi^-$ production in proton-proton collisions at $\sqrt{s}=7$ TeV, Reports No. CMS-FSQ-12-004 and No. CERN-EP-2016-261.
[4] P. Lebiedowicz, O. Nachtmann, and A. Szczurek, Central exclusive diffractive production of the $\pi^+\pi^-$ continuum, scalar and tensor resonances in pp and $p\bar{p}$ scattering within the tensor Pomeron approach, Phys. Rev. D **93**, 054015 (2016).
[5] R. Schicker (ALICE Collaboration), Central diffraction in ALICE, arXiv:1205.2588.
[6] R. McNulty, Central exclusive production at LHCb, Proc. Sci., DIS2016 (**2016**) 181.
[7] R. Sikora (STAR Collaboration), Recent results on central exclusive production with the STAR detector at RHIC, arXiv:1811.03315.
[8] R. Staszewski, P. Lebiedowicz, M. Trzebiński, J. Chwastowski, and A. Szczurek, Exclusive $\pi^+\pi^-$ production at the LHC with forward proton tagging, Acta Phys. Pol. B **42**, 1861 (2011).
[9] M. Albrow *et al.* (CMS and TOTEM Collaborations), CMS-TOTEM precision proton spectrometer, Reports No. CERN-LHCC-2014-021, No. TOTEM-TDR-003, and No. CMS-TDR-13.
[10] O. Nachtmann, Considerations concerning diffraction scattering in quantum chromodynamics, Ann. Phys. (N.Y.) **209**, 436 (1991).
[11] C. Ewerz, M. Maniatis, and O. Nachtmann, A model for soft high-energy scattering: Tensor pomeron and vector Odderon, Ann. Phys. (Amsterdam) **342**, 31 (2014).
[12] C. Ewerz, P. Lebiedowicz, O. Nachtmann, and A. Szczurek, Helicity in proton-proton elastic scattering and the spin structure of the Pomeron, Phys. Lett. B **763**, 382 (2016).
[13] L. Adamczyk *et al.* (STAR Collaboration), Single spin asymmetry A_N in polarized proton-proton elastic scattering at $\sqrt{s}=200$ GeV, Phys. Lett. B **719**, 62 (2013).
[14] P. Lebiedowicz, O. Nachtmann, and A. Szczurek, Exclusive central diffractive production of scalar and pseudoscalar mesons; tensorial vs. vectorial pomeron, Ann. Phys. (Amsterdam) **344**, 301 (2014).
[15] A. Bolz, C. Ewerz, M. Maniatis, O. Nachtmann, M. Sauter, and A. Schöning, Photoproduction of $\pi^+\pi^-$ pairs in a

model with tensor-pomeron and vector-Odderon exchange, J. High Energy Phys. 01 (2015) 151.
[16] P. Lebiedowicz, O. Nachtmann, and A. Szczurek, ρ^0 and Drell-Söding contributions to central exclusive production of $\pi^+\pi^-$ pairs in proton-proton collisions at high energies, Phys. Rev. D **91**, 074023 (2015).
[17] P. Lebiedowicz, O. Nachtmann, and A. Szczurek, Central production of ρ^0 in pp collisions with single proton diffractive dissociation at the LHC, Phys. Rev. D **95**, 034036 (2017).
[18] P. Lebiedowicz, O. Nachtmann, and A. Szczurek, Exclusive diffractive production of $\pi^+\pi^-\pi^+\pi^-$ via the intermediate $\sigma\sigma$ and $\rho\rho$ states in proton-proton collisions within tensor pomeron approach, Phys. Rev. D **94**, 034017 (2016).
[19] P. Lebiedowicz, O. Nachtmann, and A. Szczurek, Central exclusive diffractive production of $p\bar{p}$ pairs in proton-proton collisions at high energies, Phys. Rev. D **97**, 094027 (2018).
[20] P. Lebiedowicz, O. Nachtmann, and A. Szczurek, Towards a complete study of central exclusive production of K^+K^- pairs in proton-proton collisions within the tensor Pomeron approach, Phys. Rev. D **98**, 014001 (2018).
[21] P. Lebiedowicz, O. Nachtmann, and A. Szczurek, Extracting the pomeron-pomeron-$f_2(1270)$ coupling in the $pp \to pp\pi^+\pi^-$ reaction through angular distributions of the pions, arXiv:1901.07788.
[22] F. E. Close and A. Kirk, Glueball-$q\bar{q}$ filter in central hadron production, Phys. Lett. B **397**, 333 (1997).
[23] D. Barberis *et al.* (WA102 Collaboration), A kinematical selection of glueball candidates in central production, Phys. Lett. B **397**, 339 (1997).
[24] D. Barberis *et al.* (WA102 Collaboration), A study of the centrally produced $\pi^+\pi^-\pi^+\pi^-$ channel in pp interactions at 450 GeV/c, Phys. Lett. B **413**, 217 (1997).
[25] D. Barberis *et al.* (WA102 Collaboration), A study of pseudoscalar states produced centrally in pp interactions at 450 GeV/c, Phys. Lett. B **427**, 398 (1998).
[26] D. Barberis *et al.* (WA102 Collaboration), A coupled channel analysis of the centrally produced K^+K^- and $\pi^+\pi^-$ final states in pp interactions at 450 GeV/c, Phys. Lett. B **462**, 462 (1999).
[27] D. Barberis *et al.* (WA102 Collaboration), A study of the $f_0(1370)$, $f_0(1500)$, $f_0(2000)$ and $f_2(1950)$ observed in the centrally produced 4π final states, Phys. Lett. B **474**, 423 (2000).
[28] A. Kirk, Resonance production in central pp collisions at the CERN Omega spectrometer, Phys. Lett. B **489**, 29 (2000).
[29] A. Kirk, A review of central production experiments at the CERN Omega spectrometer, Int. J. Mod. Phys. A **29**, 1446001 (2014).
[30] P. S. L. Booth *et al.*, A high statistics study of the $\phi\phi$ mass spectrum, Nucl. Phys. **B273**, 677 (1986).
[31] P. S. L. Booth *et al.*, Angular correlations in the $\phi\phi$ system and evidence for hadronic η_c production, Nucl. Phys. **B273**, 689 (1986).
[32] A. Etkin, K. J. Foley, R. S. Longacre, W. A. Love, T. W. Morris, E. D. Platner, A. C. Saulys, S. J. Lindenbaum, C. S. Chan, and M. A. Kramer, Observation of three 2^{++} resonances in the glueball-enhanced channel $\pi^- p \to \phi\phi n$, Phys. Lett. **165B**, 217 (1985).
[33] A. Etkin *et al.*, Increased statistics and observation of the g_T, $g_{T'}$, and $g_{T''}$ 2^{++} resonances in the glueball enhanced channel $\pi^- p \to \phi\phi n$, Phys. Lett. B **201**, 568 (1988).
[34] D. Aston *et al.*, Strangeonia and kin: New results from kaon hadroproduction with LASS, in HADRON '89, *Proceedings of the 3rd International Conference on Hadron Spectroscopy, Ajaccio, France, 1989*, edited by F. Binon, J. M. Frere, J. P. Peigneux (Editions Frontieres, Gif-sur-Yvette, France, 1989).
[35] D. Aston *et al.*, Strangeonium production from LASS, Nucl. Phys. B, Proc. Suppl. **21**, 5 (1991).
[36] T. A. Armstrong *et al.* (ABBC Collaboration), Observation of double ϕ-meson production in the central region for the reactions $\pi^+ p \to \pi^+(K^+K^+K^-K^-)p$ and $pp \to p(K^+K^+K^-K^-)p$ at 85 GeV/c, Phys. Lett. **166B**, 245 (1986).
[37] T. A. Armstrong *et al.* (WA76 Collaboration), Observation of double ϕ-meson production in the central region for the reaction $pp \to p_f(K^+K^-K^+K^-)p_s$ at 300 GeV/c, Phys. Lett. B **221**, 221 (1989).
[38] D. Barberis *et al.* (WA102 Collaboration), A study of the centrally produced $\phi\phi$ system in pp interactions at 450 GeV/c, Phys. Lett. B **432**, 436 (1998).
[39] C. Evangelista *et al.* (JETSET Collaboration), Study of the reaction $\bar{p}p \to \phi\phi$ from 1.1 to 2.0 GeV/c, Phys. Rev. D **57**, 5370 (1998).
[40] D. Bisello *et al.* (DM2 Collaboration), Search of glueballs in the $J/\psi \to \gamma\phi\phi$ decay, Phys. Lett. B **179**, 294 (1986).
[41] Z. Bai *et al.* (MARK III Collaboration), Observation of a Pseudoscalar State in $J/\psi \to \gamma\phi\phi$ near $\phi\phi$ Threshold, Phys. Rev. Lett. **65**, 1309 (1990).
[42] M. Ablikim *et al.* (BES Collaboration), Partial wave analysis of $J/\psi \to \gamma\phi\phi$, Phys. Lett. B **662**, 330 (2008).
[43] M. Ablikim *et al.* (BESIII Collaboration), Observation of pseudoscalar and tensor resonances in $J/\psi \to \gamma\phi\phi$, Phys. Rev. D **93**, 112011 (2016).
[44] C. J. Morningstar and M. J. Peardon, Efficient glueball simulations on anisotropic lattices, Phys. Rev. D **56**, 4043 (1997).
[45] C. J. Morningstar and M. J. Peardon, Glueball spectrum from an anisotropic lattice study, Phys. Rev. D **60**, 034509 (1999).
[46] A. Hart and M. Teper (UKQCD Collaboration), On the glueball spectrum in $O(a)$-improved lattice QCD, Phys. Rev. D **65**, 034502 (2002).
[47] M. Loan, X.-Q. Luo, and Z.-H. Luo, Monte Carlo study of glueball masses in the Hamiltonian limit of SU(3) lattice gauge theory, Int. J. Mod. Phys. A **21**, 2905 (2006).
[48] E. Gregory, A. Irving, B. Lucini, C. McNeile, A. Rago, C. Richards, and E. Rinaldi, Towards the glueball spectrum from unquenched lattice QCD, J. High Energy Phys. 10 (2012) 170.
[49] Y. Chen *et al.*, Glueball spectrum and matrix elements on anisotropic lattices, Phys. Rev. D **73**, 014516 (2006).
[50] W. Sun, L.-C. Gui, Y. Chen, M. Gong, C. Liu, Y.-B. Liu, Z. Liu, J.-P. Ma, and J.-B. Zhang, Glueball spectrum from $N_f = 2$ lattice QCD study on anisotropic lattices, Chin. Phys. C **42**, 093103 (2018).

[51] R. S. Longacre and S. J. Lindenbaum, Evidence for a fourth state related to the three $J^{PC} = 2^{++}$, $\pi^- p \to \phi\phi n$ states explainable by 2^{++} glueball production, Phys. Rev. D **70**, 094041 (2004).

[52] Y.-B. Yang, L.-C. Gui, Y. Chen, C. Liu, Y.-B. Liu, J.-P. Ma, and J.-B. Zhang (CLQCD Collaboration), Lattice Study of Radiative J/ψ Decay to a Tensor Glueball, Phys. Rev. Lett. **111**, 091601 (2013).

[53] M. Ablikim *et al.* (BESIII Collaboration), Partial wave analysis of $J/\psi \to \gamma\eta\eta$, Phys. Rev. D **87**, 092009 (2013); Erratum, Phys. Rev. D **87**, 119901(E) (2013).

[54] M. Ablikim *et al.* (BESIII Collaboration), Amplitude analysis of the $K_S K_S$ system produced in radiative J/ψ decays, Phys. Rev. D **98**, 072003 (2018).

[55] M. Tanabashi *et al.* (Particle Data Group), Review of particle physics, Phys. Rev. D **98**, 030001 (2018).

[56] P. Lebiedowicz and A. Szczurek, Exclusive $pp \to pp\pi^+\pi^-$ reaction: From the threshold to LHC, Phys. Rev. D **81**, 036003 (2010).

[57] R. A. Kycia, J. Chwastowski, R. Staszewski, and J. Turnau, GenEx: A simple generator structure for exclusive processes in high energy collisions, Commun. Comput. Phys. **24**, 860 (2018).

[58] R. A. Kycia, J. Turnau, J. J. Chwastowski, R. Staszewski, and M. Trzebiński, The adaptive Monte Carlo toolbox for phase space integration and generation, Commun. Comput. Phys. **25**, 1547 (2019).

[59] R. Kycia, P. Lebiedowicz, A. Szczurek, and J. Turnau, Triple Regge exchange mechanisms of four-pion continuum production in the $pp \to pp\pi^+\pi^-\pi^+\pi^-$ reaction, Phys. Rev. D **95**, 094020 (2017).

[60] A. Donnachie and P. V. Landshoff, Total cross sections, Phys. Lett. B **296**, 227 (1992).

[61] A. Donnachie, H. G. Dosch, P. V. Landshoff, and O. Nachtmann, Pomeron physics and QCD, Cambridge Monogr. Part. Phys., Nucl. Phys., Cosmol. **19**, 1 (2002).

[62] M. Derrick *et al.* (ZEUS Collaboration), Measurement of elastic ϕ photoproduction at HERA, Phys. Lett. B **377**, 259 (1996).

[63] J. Breitweg *et al.* (ZEUS Collaboration), Measurement of diffractive photoproduction of vector mesons at large momentum transfer at HERA, Eur. Phys. J. C **14**, 213 (2000).

[64] P. D. B. Collins, *An Introduction to Regge Theory and High Energy Physics* (Cambridge University Press, Cambridge, England, 1977).

[65] L. A. Harland-Lang, V. A. Khoze, and M. G. Ryskin, Modelling exclusive meson pair production at hadron colliders, Eur. Phys. J. C **74**, 2848 (2014).

[66] C. Ewerz, The Odderon in quantum chromodynamics, arXiv:hep-ph/0306137.

[67] L. Łukaszuk and B. Nicolescu, A possible interpretation of pp rising total cross-sections, Lett. Nuovo Cimento **8**, 405 (1973).

[68] D. Joynson, E. Leader, B. Nicolescu, and C. Lopez, Non-regge and hyper-regge effects in pion-nucleon charge exchange scattering at high energies, Nuovo Cimento Soc. Ital. Fis. **30A**, 345 (1975).

[69] G. Antchev *et al.* (TOTEM Collaboration), First determination of the ρ parameter at $\sqrt{s} = 13$ TeV—probing the existence of a colourless three-gluon bound state, Report No. CERN-EP-2017-335.

[70] G. Antchev *et al.* (TOTEM Collaboration), Elastic differential cross-section $d\sigma/dt$ at $\sqrt{s} = 2.76$ TeV and implications on the existence of a colourless 3-gluon bound state, Reports No. CERN-EP-2018-341 and No. TOTEM-2018-002.

[71] E. Martynov and B. Nicolescu, Did TOTEM experiment discover the Odderon?, Phys. Lett. B **778**, 414 (2018).

[72] E. Martynov and B. Nicolescu, Evidence for maximality of strong interactions from LHC forward data, Phys. Lett. B **786**, 207 (2018).

[73] V. A. Khoze, A. D. Martin, and M. G. Ryskin, Elastic proton-proton scattering at 13 TeV, Phys. Rev. D **97**, 034019 (2018).

[74] M. Broilo, E. Luna, and M. Menon, Forward elastic scattering and Pomeron models, Phys. Rev. D **98**, 074006 (2018).

[75] V. P. Goncalves, Searching the Odderon in the diffractive $f_2(1270)$ photoproduction at pA collisions, arXiv:1811.07622.

[76] L. A. Harland-Lang, V. A. Khoze, A. D. Martin, and M. G. Ryskin, Searching for the Odderon in ultraperipheral proton-ion collisions at the LHC, Phys. Rev. D **99**, 034011 (2019).

[77] T. Csörgő, R. Pasechnik, and A. Ster, Odderon and proton substructure from a model-independent Lévy imaging of elastic pp and $p\bar{p}$ collisions, Eur. Phys. J. C **79**, 62 (2019).

[78] A. Schäfer, L. Mankiewicz, and O. Nachtmann, Double-diffractive J/ψ and ϕ production as a probe for the Odderon, Phys. Lett. B **272**, 419 (1991).